Renewable Energy 200 (2022) 1393–1415

Contents lists available at ScienceDirect

Renewable Energy

journal homepage: www.elsevier.com/locate/renene

# Experimental investigation on the dynamic response of an innovative semi-submersible floating wind turbine with aquaculture cages

Shugang Cao [a,b], Youliang Cheng [a,**], Jinlong Duan [c,*], Xiaoxu Fan [b]

[a] Hebei Key Laboratory of Low Carbon and High Efficiency Power Generation Technology, Department of Power Engineering, North China Electric Power University, Baoding, 071003, China
[b] Longyuan Power Group Co., Ltd., Beijing, 100034, China
[c] CAS Key Laboratory for Mechanics in Fluid Solid Coupling Systems, Institute of Mechanics, Beijing, 100190, China

ARTICLE INFO

*Keywords:*
Model test
Semi-submersible floating wind turbine
Aquaculture cage
Dynamic response
Various environmental conditions

ABSTRACT

Floating offshore wind turbines integrating with other functional devices can not only produce green electricity but also realize three-dimensional utilization of ocean space. Therefore, an innovative concept of semi-submersible floating wind turbine with aquaculture cages is proposed here. Correspondingly, its dynamical behaviors are required to be examined and investigated while various oceanic conditions are considered, including but not limited to an irregular wave condition and combined wind and wave conditions. Hence, a series of model tests in 1:40 scale is carried out in Shanghai Jiao Tong University Ocean Engineering Basin. Firstly, the scaling law and experimental setup are interpreted in detail. Calibrations of the wind generator and wave makers are carefully performed to ensure the accuracy and reliability of model tests. Then the dynamic responses of the new floating wind-aquaculture platform (FWAP) are studied experimentally, including the periods, damping, motions, accelerations and tower top loads. The results show that the existence of nets mainly has a damping effect on the dynamics of the new FWAP under different sea states. The motions, accelerations and tower top loads can be significantly increased when the FWAP undergoes 50-year extreme sea state. When the new FWAP is subjected to combined wind and wave, more complicated dynamic responses can be detected due to the rotation of wind turbine. The results can serve as a reference basis for the improvement of the new FWAP.

## 1. Introduction

Since clean energy, such as solar, wind and tidal energy, is environmentally friendly and scarcely depleted, innovative concepts have been recently proposed to harvest these types of energy so as to ameliorate the shortage of energy. Among these inventions, offshore wind turbine concepts have been widely advocated and utilized for the harvest of wind energy in the ocean, which can be categorized into fixed and floating offshore wind turbines. Fixed offshore wind turbines are mostly designed and applied in coastal waters along the shoreline while floating offshore wind turbines (FOWT) can serve in the ocean with depth of more than 50 m. Therefore, plenty of new concepts of FOWT have been emerging over years. Noteworthy is that FOWT is inevitably subjected to complicated oceanic conditions when serving in deep water, making it very significant to ensure the safety of FOWT. Therefore, the dynamics and behaviors of FOWT need to be assessed before FOWT is put into service. Correspondingly, great efforts have been made to the investigations on the dynamics of FOWT, experimentally and numerically. Among these approaches, experimental approaches are commonly regarded as an effective method to reproduce and capture the complicated and strongly nonlinear responses of FOWT related to numerous variables. It should also be noticed that it is not financially viable to conduct experiments of FOWT in full scale. Therefore, experimental researches on dynamic responses of FOWT models with certain scale ratios have been carried out by many investigators recently so that the complex behaviors of FOWT can be investigated and assessed. These test results have laid solid foundations for FOWT design in the actual oceanic environment.

For decades, FOWT model tests with various types of floating foundations, such as spar, semi-submersible and TLP concepts, have been attempted and performed. For example, experimental studies of the spar-buoy FOWT were carried out by Nielsen et al. [1] and Tomasicchio

* Corresponding author.
** Corresponding author.
*E-mail addresses:* ylcheng001@163.com (Y. Cheng), duanjl@imech.ac.cn (J. Duan).

https://doi.org/10.1016/j.renene.2022.10.072
Received 19 May 2022; Received in revised form 13 October 2022; Accepted 15 October 2022
Available online 18 October 2022

et al. [2], wherein the structural dynamics was examined under both wind and wave loads, including the motion, acceleration and forces under various environmental conditions. Besides the spar buoy offshore wind turbine, a 1:67 scale model test of the semi-submersible WindFloat concept with a three-legged floater was conducted by Roddier et al. [3]. Based on the experimental data, a simplified aerodynamic model of the wind turbine was proposed and the accuracy of the numerical model was examined for engineering design. Similarly, a trimmed floater of a semi-submersible wind turbine was also modelled to examine the variation of nonlinear wave loads during operation of a floating wind turbine by Li and Bachynski [4], in order to validate the developed model based on potential-flow theory with Morison type drag. In addition to combined wind and wave conditions, current was also included while the model tests of a semi-submersible FOWT in 1:50 scale was performed by Hsu et al. [5]. In their research, the drift force induced by wind and the drag force led by current were particularly focused on. A semi-submersible FOWT with trussed slender structures was designed and studied by Liu et al. [6,7] experimentally and numerically. It was found that the translational surge or sway motion could be significantly excited at its resonance frequency in steady wind. The hydrodynamic performance of two semi-submersible platforms with three and four columns supporting a vertical axis wind turbine was also studied through basin tests by Rajeswari et al. [8], in which the heave and roll responses of these two types of FOWT were compared and discussed. In order to explore the dynamic responses of FWOT with various floating concepts (spar-buoy, TLP and semi-submersible foundations) thoroughly, the behaviors of models in 1:50 scale were studied in the Maritime Research Institute Netherlands (MARIN) by Goupee et al. [9], Koo et al. [10], Martin et al. [11], Martin 12] and Robertson et al. [13]. During the tests, the thrust force exerted on the wind turbine was generated by a designed wind generator. The performances of FOWT with three types of foundations were analyzed and compared, including the global motions, tower dynamics and the mooring system response. Likewise, collaborative model tests of three FOWT concepts were also conducted by four universities in Japan. The experimental results were presented by Nihei et al. [14], in which the motion performance in terms of motion response amplitude operators (RAOs) was mainly focused under different oceanic conditions. By considering coupling of wind and wave, model tests of TLP FOWT in 1:100 scale were also carried out by Nihei and Fujioka [15], wherein the floater pitch motion and mooring line vibrations were found decreased by the blade-wind interaction. Besides, the hydrodynamic performance of a TLP FOWT was also experimentally researched by Rodriguez et al. [16]. Responses including regular wave motion, irregular wave responses, tendon loads and accelerations were mainly monitored and analyzed. In order to compare two types of blade system, OC3-Hywind FOWT was experimentally investigated by Duan et al. [17,18]. Similar response characteristics of FOWT were observed under various environmental conditions. All these experimental investigations on dynamics of FOWT can provide supportive theory and experience for the commercial application of FOWT in future.

Although FOWT technology can ameliorate the energy shortage caused by social development, the developing cost of FOWT is still an issue worthy attention, making it difficult for the commercial application of FOWT now. Recently, great efforts have been made to either reduce the developing cost of FOWT or improve the economic efficiency of FOWT so that the profitability of FOWT can be maximized. The former concept mainly includes to decrease the usage amount of steel or conduct efficient transportation and installation. While the latter one provides new concepts of FOWT combining with wave energy converters or fish farming cages [19–25]. Moreover, the commercial application of the first semi-submersible fish farm in Norway, Ocean Farm1, has proved the feasibility and viability of realizing combination structure integrating FOWT and fish farming cages [26]. Correspondingly, investigations on such concepts of complicated FOWT have been emerged. For instance, an innovative structure integrating a floating offshore wind turbine with a steel fish farming cage (FOWT-SFFC) was designed by Zheng and Lei [27], which is mainly composed of a floating wind turbine and an octagonal fish cage in the foundation. The dynamic responses of FOWT-SFFC were firstly studied numerically [27–29], and then examined experimentally by Lei et al. [30], wherein dynamic characteristics like the tower vibration frequencies, the stiffness of the mooring system, hydrodynamic damping and RAOs were analyzed and discussed under various environmental conditions. Besides, a novel concept by combining fish cages and spar type wind turbine was also proposed and developed by Chu and Wang [31,32], in which the interaction between the floating structure and mooring lines was researched based on the potential flow theory with considering the effect of fish nets. A new concept of a floating vertical-axis wind turbine (VAWT) combining with a steel fishing cage was also designed by Zheng et al. [33]. Then the kinetic characteristics of this floater were probed experimentally.

As new concepts of FOWT combining with fish cages can be utilized to tackle energy shortage in future efficiently and economically, their dynamic responses and characteristics should be investigated and understood thoroughly and comprehensively so that the safety of this new type of equipment can be guaranteed. Nonetheless, new concepts of FOWT combining with aquaculture cages are very limited currently, and their accordant experimental investigation is still insufficient. Therefore, more innovative concepts of FOWT combining with fish nets should be developed, and more model tests of FOWT combining with fish cages should be carried out, so as to provide a reliable reference for the design of FOWT combining with aquaculture cages. Correspondingly, as shown in Fig. 1, a new concept of an innovative semi-submersible floating wind turbine with aquaculture cages is proposed here and the dynamic behaviors of the new floating wind-aquaculture platform (FWAP) in 1:40 scale is investigated experimentally under various environmental conditions in our work. In addition, the effect of aquaculture nets on dynamic responses of the new FWAP is examined based on the comparison between dynamics of the new FWAP without and with nets. Compared with the existing ones [27–33], the semi-submersible foundation of the new FWAP is in the form of three columns with triangular arrangement, wherein the upper section of each column is invertedly designed in order to avoid the influence of wave effectively. Regarding to the lower section of each column, a

**Fig. 1.** Schematic illustration of the concept of the new FWAP.

large-diameter ballast tank is directly applied to increase the hydrodynamic damping of the foundation so that the safety of the whole FWAP can be guaranteed.

It should be emphasized that the novelty of our work is to examine the dynamic behavior of a new concept of FWAP under different environmental conditions, which can provide a reference basis for the scheme design and theoretical calculation of the new FWAP. The paper is structured as follows. In Section 2, the physical model of the new FWAP, scaling law, experimental setup and implementation are elaborated. Then the wave maker and wind generator are calibrated in Section 3. Experimental results of the new FWAP without or with nets are presented and analyzed in Section 4, including the periods, damping, motions, accelerations and tower top loads. Based on the results, discussion is made in the following section. Finally, conclusions are drawn.

## 2. Experimental setup

In order to obtain the dynamic characteristics of the coupling of aerodynamic, hydrodynamic and structural responses under different environmental conditions, a systematic basin model test of the new FWAP is carried out in a wind-wave basin. Some key performance parameters of the FWAP are tested and analyzed, such as natural period, damping, RAOs, motion performance, acceleration, tower top load, etc. Through basin model test, the design of aerodynamic force, hydrodynamics, structural dynamics and the coupling dynamic performance can be researched and evaluated for the supporting platform, which can provide references for further in-depth study. The contents of the model test mainly include: a) Still water decay test, wherein the natural period and damping coefficient of the FWAP system can be obtained; b) Wind and wave test under working and survival conditions, wherein the motion response of the FWAP system, acceleration and tower top load can be examined.

### 2.1. Marine engineering basin

The model tests of the new FWAP are conducted in Shanghai Jiao Tong University ocean engineering basin, where various marine environmental conditions such as wind and wave can be simulated. The main scale of the pool is 50m × 30m × 6m, and the main equipment of the test facilities and instruments includes wave making and suppression systems, wind generating system, non-contact 6-DOF motion measuring instrument, all kinds of measuring instruments and meters as well as automatic data acquisition and real-time analysis system. The wave making system is equipped with a German Kempf & Remmers double push plate high power hydraulic wave making machine, and can produce regular wave or irregular wave, long peak wave. The maximum wave height is up to 0.5m. The wind generating system consists of a set of movable axial flow fan wind generating system, which can generate steady wind or wind spectrum (unsteady wind) in any direction in the pool, with the maximum wind speed 10 m/s.

### 2.2. Instrumentation

In order to acquire the dynamic behavior of the new FWAP accurately, various types of test and data acquisition instruments are used in this model test. One set of non-contact optical 6-DOF motion measurement system is applied to measure the 6-DOF motion at the center of gravity of the FWAP in wind and wave tests. Two motion acceleration sensors are utilized to monitor the longitudinal, transverse and vertical motion acceleration of the new FWAP at the center of gravity of nacelle and platform, while one six-component force sensor is used to measure the longitudinal, transverse and vertical force and bending moment of the FWAP at the top of the tower. Some of the sensor arrangements described in this section can be found in the model photos in section 2.4. In addition, the wind and wave conditions are also monitored by specific instruments to ensure the model tests to be conducted under certain environmental conditions. During model tests, one hot film wind speed sensor is applied to measure, calibrate and collect the simulated wind speed. Five sets of capacitive wave height meter are used to monitor the relative wave surface elevation at the typical position of FWAP, and to measure the wave height and period in the process of ocean environment simulation. Moreover, one digital camera and two digital HD cameras are used for shooting all test conditions and test process.

For quality assurance during the model tests, the above test instruments and data acquisition system have been rigorously calibrated and checked before the formal test of this project to ensure the accuracy and reliability of the measured data in the experiments.

### 2.3. Scaling law

It is important to seek the appropriate scaling law before the implementation of model tests. Froude number similarity can guarantee the correct similarity of gravity and inertia forces between model and entity. The prototype and the model must meet the same ratio of the rotor thrust to the gravity of the structure. That is, the prototype and the model must ensure the same thrust coefficient of the wind wheel. Tip speed ratio (TSR) similarity can ensure that the rotor rotation speed, system excitation frequency due to rotor imbalance and the aerodynamic interaction between tower and blade of the model structure are similar to those of the prototype. While the similarity of structural stiffness can guarantee that the natural frequency and deformation of the model structure are designed according to those of the prototype.

Although Reynolds number similarity and Froude number similarity are typically used for a fluid flow and gravity waves respectively, it has been proved that seeking balance of these two numbers for the scaled model test of a FOWT is almost impossible at the same time [34]. When wave force and inertial effects are dominated, the Froude number similarity is commonly employed in the model test of a FOWT [12]. Therefore, based on Froude number similarity, the physical model of the new FWAP in scale 1:40 is designed. Correspondingly, the conversion relationship of various physical quantities between the model and prototype is presented in Table 1.

### 2.4. Experimental models

The new FWAP is mainly composed of four parts: wind turbine system (Rotor-Nacelle-Assembly, RNA), tower, semi-submersible support platform and nets, as shown in Fig. 2. The wind turbine system is arranged on the top of the tower while the tower is located in the middle of the whole FWAP system, and the lower part is a semi-submersible support platform. The supporting platform consists of three uniformly distributed circular circumferential columns, transverse bracing, diagonal bracing, heave plate and mooring system. Aquaculture nets are installed on the side and bottom of the floating platform to form a breeding space.

According to the main scale of the new FWAP and the facility

**Table 1**
The conversion relationship of various physical quantities between the model and prototype.

| Parameter | Symbol | Scaling factor |
|---|---|---|
| Length | $L_s/L_m$ | $\lambda$ |
| Linear velocity | $v_s/v_m$ | $\lambda^{1/2}$ |
| Linear acceleration | $a_s/a_m$ | 1 |
| Angle | $\varphi_s/\varphi_m$ | 1 |
| Angular velocity | $\varphi_s'/\varphi_m'$ | $\lambda^{-1/2}$ |
| Period | $T_s/T_m$ | $\lambda^{1/2}$ |
| Density | $\rho_s/\rho_m$ | $\gamma$ |
| Mass | $\Delta_s/\Delta_m$ | $\gamma\lambda^3$ |
| Rotor thrust | $F_s/F_m$ | $\lambda^3$ |
| Rotor moment | $M_s/M_m$ | $\lambda^4$ |
| Elastic modulus | $E_s/E_m$ | $\lambda$ |

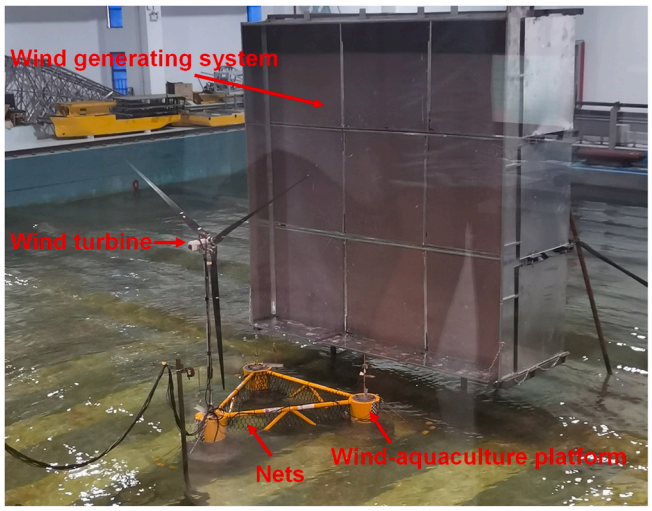


**Fig. 2.** Model of the new FWAP in ocean basin.

conditions for model test of the ocean engineering basin, the scaling factor λ of the model is taken as 40. The actual water depth at the location of the prototype wind turbine is 35m, so the water depth in the model test is 0.875m. The layout of wind generation system, experimental model, mooring system, etc. in the pool is shown in Fig. 3.

#### 2.4.1. Modelling of the wind turbine

The prototype of wind turbine system (RNA) is a 4-MW wind turbine, which is a three-blade upwind turbine. The main parameters of the model wind turbine are obtained according to the scaling laws. As shown in Fig. 4, the main metal parts of the model wind turbine, including nacelle and hub, are made of high-strength aluminum alloy by CNC, so as to minimize the weight of the model wind turbine to meet the weight similarity relationship and meet the requirements of strength and stiffness. The model blades are made of carbon fiber to meet the weight similarity relationship. The main parameters of the prototype 4 MW wind turbine and model turbine are shown in Table 2.

#### 2.4.2. Modelling of the tower

The model tower is a shell type variable section structure. Aluminum alloy 2024 is used as the material of the model tower. The model tower length is determined after considering the height of upper and lower sensors and connected parts in order to meet the target hub center height of the model. In order to meet the requirements of the total weight of the tower, by considering the weight of the upper and lower sensors of the tower, the weight of the connected parts and the sensor data acquisition cable, the weight of the model tower are carefully adjusted. The model tower and its parameters are shown in Fig. 5 and Table 3.

#### 2.4.3. Modelling of the semi-submersible platform

The main body of the semi-submersible platform is made of wood materials and 3D resin printed components, and the connection and support between the columns are made of carbon fiber pipes. Watertight materials are used to seal the joints of the model to prevent water seepage on the platform. A certain space is reserved inside to place the ballast, which is used to adjust the model weight, the center of gravity position, and the radius of roll and pitch inertia. The geometric scale of all model components is determined according to the scaling ratio of the model, and the error of the geometric scale of the model is less than 1 mm. The parameters of the semi-submersible platform model, such as displacement, center of gravity position, pitch and roll inertia radius, are adjusted by adding or changing the mass and position of ballast in the main space of the semi-submersible platform model.

The main scale and main parameters of the semi-submersible lower floating body model of the new FWAP are shown in Fig. 6 and Table 4.

#### 2.4.4. Modelling of the mooring system

The mooring system is composed of three groups of mooring cable, and the angle between each group of mooring cables is 120°. Each group of mooring cables contains 3 mooring cables, and the angle between the mooring cables in the same group is 5°, as shown in Fig. 9. Each mooring cable is composed of chain, floater and clump weight, and is respectively connected to the top of the semi-submersible floating platform and the anchor point located on the seabed (Figs. 7 and 8). Due to the shallow water mooring design in this project, the prototype design water depth is 35m, and the simulated water depth under the condition of 1:40 scale ratio can meet the similar relationship, so there is no need to carry out the design of water depth truncated mooring system. In the mooring system layout shown in Figs. 7 and 9, the origin of coordinates is located at the triangular centroid of the static water surface, and the coordinates of fairlead and anchor points are given accordingly, as shown in Table 5.

#### 2.4.5. Modelling of the fish nets

The covering nets around the semi-submersible floating body is used for aquaculture fishery. The covering nets mainly consists of three side nets and one bottom net. The nets used in the experiment was a full-size tortoise shell net. The size of the nets model is shown in the Table 6.

### 2.5. Coordinate systems

This model test involves three coordinate systems: the geodetic coordinate system (global coordinate system), the platform body coordinate system and the nacelle local coordinate system, as shown in Fig. 10.

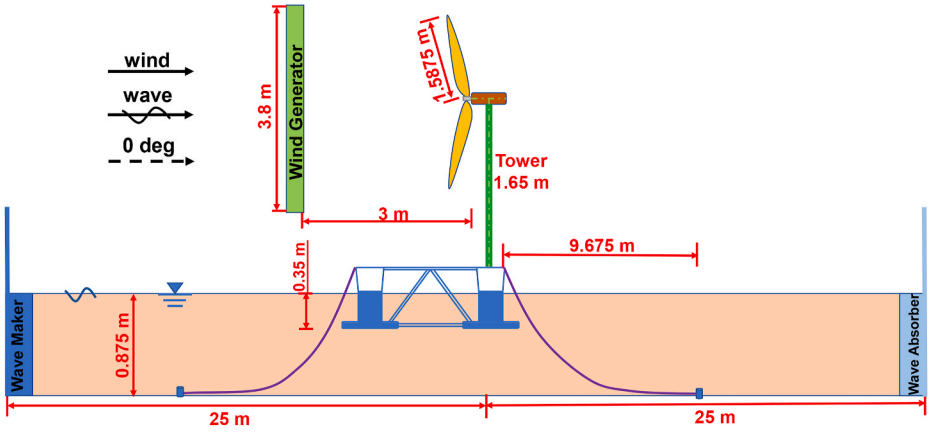


**Fig. 3.** Test arrangement in the wind-wave basin.

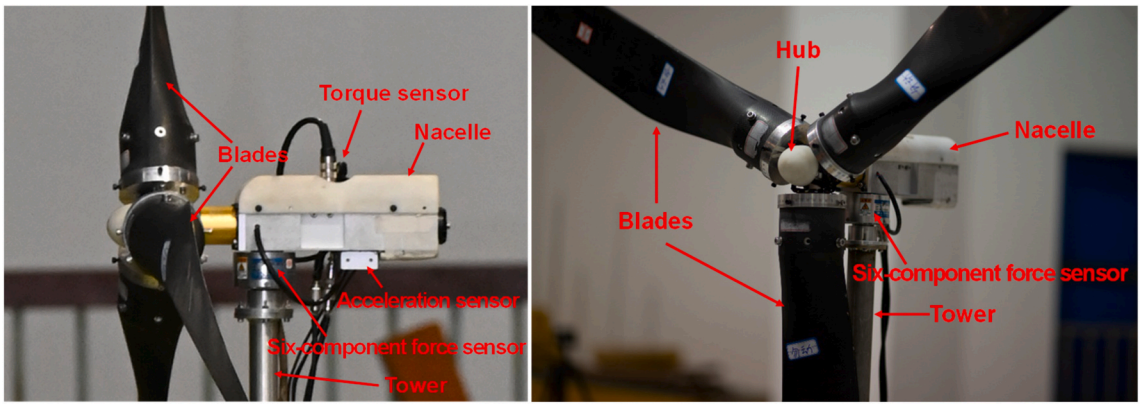


**Fig. 4.** Model of the wind turbine.

**Table 2**
Main parameters of the 4-MW wind turbine.

| Parameters | Unit | Prototype value | Model value |
|---|---|---|---|
| Rotor diameter | m | 130 | 3.25 |
| Hub height | m | 85.213 | 2.130 |
| Mass of RNA | kg | 239,201 | 3.7375 |
| Rated wind speed | m/s | 10.5 | 1.66 |
| Rated rotor speed | rpm | 13.36 | 84.496 |
| Rated rotor thrust | N | 712,400 | 11.131 |

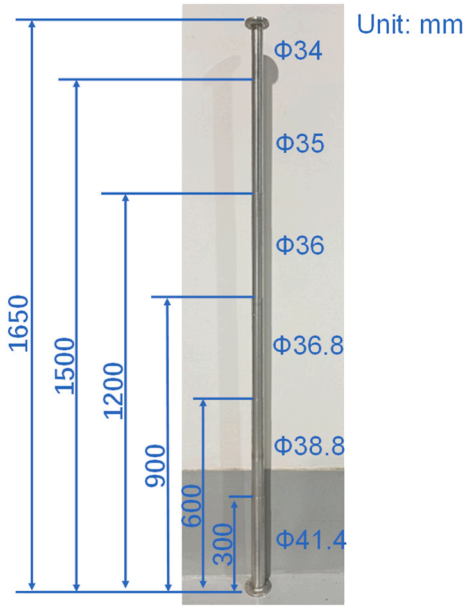


**Fig. 5.** Model of the tower.

**Table 3**
Main parameters of the prototype tower and model tower.

| Parameters | Unit | Prototype value | Model value |
|---|---|---|---|
| Length | m | 73 | 1.825 |
| Mass | kg | 338,390 | 5.287 |
| Height of the CG | m | 25.5 | 0.625 |
| 1st FA natural frequency | Hz | 0.5497 | 3.480 |
| 1st SS natural frequency | Hz | 0.5397 | 3.410 |

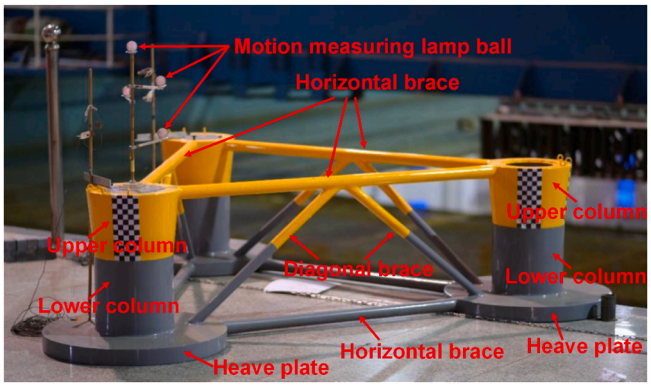


**Fig. 6.** Model of the semi-submersible lower floating body of the new FWAP.

**Table 4**
Main scale and main parameters of the semi-submersible platform.

| Parameters | Unit | Prototype value | Model value |
|---|---|---|---|
| Column spacing | m | 70 | 1.750 |
| Diameter of upper columns | m | 14 | 0.350 |
| Diameter of lower columns | m | 12 | 0.300 |
| Diameter of heave plates | m | 28 | 0.700 |
| Diameter of horizontal braces | m | 2 | 0.050 |
| Diameter of diagonal braces | m | 1.6 | 0.040 |
| Designed draft | m | 14 | 0.350 |
| Displacement | kg | 9376,000 | 142.930 |
| COG-X (ballast included) | m | 20.301 | 0.508 |
| COG-Y (ballast included) | m | 0.0346 | 0.001 |
| COG-Z (ballast included) | m | 10.912 | 0.273 |
| Rxx (ballast included) | m | 34.620 | 0.866 |
| Ryy (ballast included) | m | 34.884 | 0.872 |
| Rzz (ballast included) | m | 40.729 | 1.018 |

Among them, the definition of the geodetic coordinate system stipulates that the due north direction is 0° (Fig. 9). The incidence angles of wind and wave are defined according to the geodetic coordinate system. In addition, for the body coordinate system *O-XYZ* of the FWAP, the *X* axis is positive pointing to the tower-column. The *Z* axis is positive vertically upward, and the *Y* axis is defined by the right hand rule. The origin of the body coordinate system is at the center of gravity of the FWAP, and its complex motion at any time can be decomposed into six degrees of freedom motion, namely three linear displacements (surge, sway and heave) and three angular displacements (roll, pitch and yaw). In this test, the 6-DOF motion of the FWAP follows the definition of the platform body coordinate system. The origin of the nacelle local coordinate system is at the intersection of the center line of the tower cylinder and the turbine shaft axis. The *X* axis points to the tail of the nacelle, that is,

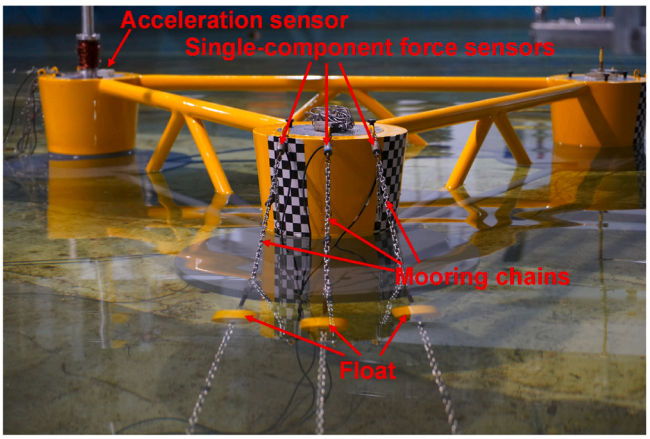


**Fig. 7.** Cable models in water.

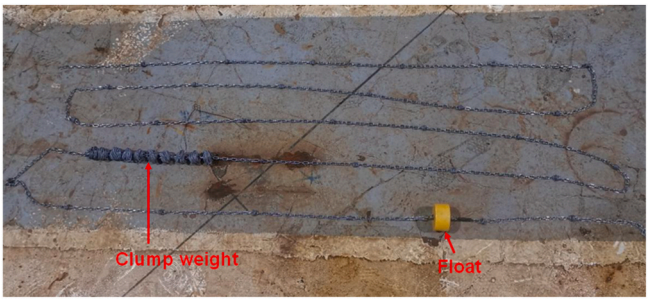


**Fig. 8.** Model of the mooring cable.

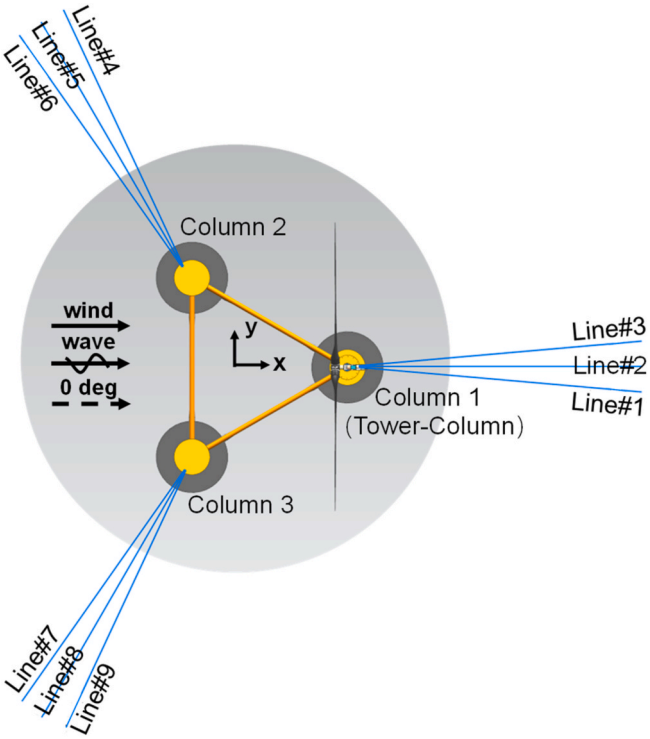


**Fig. 9.** Schematic diagram of the mooring system.

**Table 5**
Mooring system characteristic parameters and physical characteristics.

| Parameters | Unit | Prototype value | Model value |
|---|---|---|---|
| Air weight linear density | kg/m | 311.47 | 0.1947 |
| Unstretched length | m | 400 | 10 |
| Initial horizontal span | m | 387 | 9.675 |
| Axial stiffness (EA) | kN | 1.16E+06 | 1.82E+01 |
| Pretension | kN | 330.63 | 0.0052 |
| Fairlead point height (to MSL) | m | 10 | 0.25 |
| The number of float | – | 9 | 9 |
| Float volume | $m^3$ | 10 | 0.0001563 |
| Float weight in air | ton | 3 | 4.688E-05 |
| The number of clump weight | – | 90 | 90 |
| Clump weight | ton | 10 | 1.563E-04 |

the downwind direction is positive; the *Z* axis points straight up, and the *Y* axis is defined by the right hand rule. In this work, the data such as the load on the top of the tower follow the definition of the nacelle local coordinate system.

### 2.6. Test implementation

Firstly, the coordinate and position of anchor are determined in the pool. The overall water depth of the pool is then adjusted to the specified water depth to the required simulation by rising or dropping the large area false bottom. Thereafter, the new FWAP, anchor chain and nets, as well as related measuring instruments, shall be installed and arranged in the pool according to the test scheme. After the instrument is installed in place, start the wave maker to generate the required waves.

The real-time data acquisition system controlled by computers is used to collect and record the test data, and the real-time data analysis and processing are carried out. The data sampling frequency is 40 Hz. Among them, the data sampling time of irregular wave test is not less than 28.5 min, corresponding to the full-size time of 3 h, and the sampling point is not less than 68400 points. At the beginning of each irregular wave test, there is an interval of 1.5 min from the beginning of wave making instructions to the beginning of formal sampling records, so as to ensure that the FWAP model is in a stable motion state when the formal test data is sampled, in order to eliminate the interference caused by the initial motion state.

### 2.7. Test setup and conditions

The basin model tests of the new FWAP include aerodynamic performance calibration test of the model wind turbine, static water test, wave test, combined wind and wave test, etc.

#### 2.7.1. Still water tests

The still water test conditions of the new FWAP mainly refer to the still water decay test (see Table 7). The still water decay test includes the respective decay test of the new FWAP without or with nets itself in the 3 DOF (heave, pitch and roll) for free-floating body and 6 DOF after attaching the mooring system. The purpose of the test is to measure the natural motion period and linear damping coefficient of the new FWAP and the same data after the coupling of the platform and the anchor system through the free vibration in a certain direction of motion of the new FWAP. Thus, the intrinsic properties of the system are obtained.

#### 2.7.2. White noise wave tests

The white noise wave test includes turbine + platform + mooring system, turbine + platform + mooring system + nets under 0° wave direction, as shown in Table 8. The white noise test condition is intended to quickly obtain the frequency responses of the platform motion under wave, including the amplitude response operators RAOs of the response, to check and analyze the test results under the irregular waves and to analyze the effect of non-linearity.

**Table 6**
Net characteristic parameters.

| Side net dimension | | Bottom net dimension | | Actual net mesh dimension | | |
|---|---|---|---|---|---|---|
| Length-L | Width-H | Length-L | Width-H | Size-a | Size-b | Diameter-c |
| 1375 mm | 500 mm | 1375 mm | 101 mm | 71 mm | 51 mm | 3 mm |

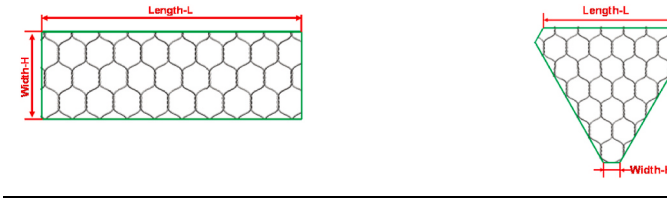


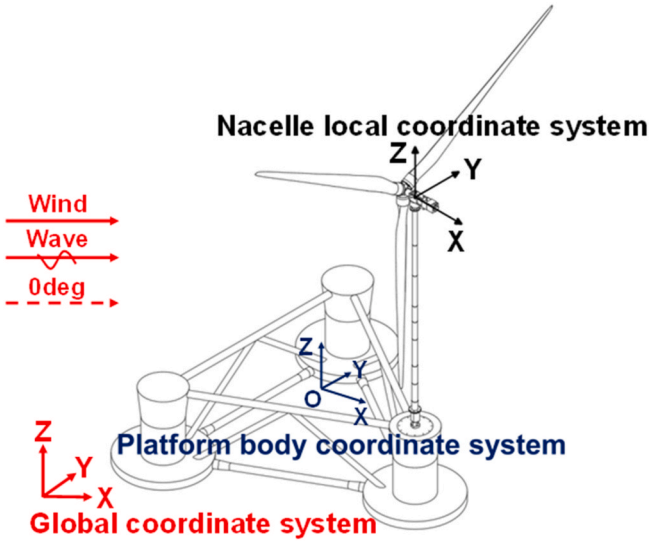


**Fig. 10.** Coordinate systems of the new FWAP.

**Table 7**
Still water test conditions.

| Configuration | Items |
|---|---|
| turbine + platform | Heave, pitch, roll |
| turbine + platform + nets | Heave, pitch, roll |
| turbine + platform + mooring system | Heave, pitch, roll, surge, sway, yaw |
| turbine + platform + mooring system + nets | Heave, pitch, roll, surge, sway, yaw |

**Table 8**
White noise wave test conditions.

| Configuration | Prototype | | Model | |
|---|---|---|---|---|
| | Hs (m) | Tp (s) | Hs (m) | Tp (s) |
| turbine + platform + mooring system<br>turbine + platform + mooring system + nets | ~2 | 5–25 | ~0.05 | 0.125–0.625 |

**Table 9**
Irregular wave test conditions.

| Sea states | Prototype | | | Model | | |
|---|---|---|---|---|---|---|
| | Hs (m) | Tp (s) | γ | Hs (m) | Tp (s) | γ |
| Rated | 0.9786 | 5.9463 | 1 | 0.024 | 0.940 | 1 |
| Cut out | 3.4421 | 7.4106 | 1 | 0.086 | 1.172 | 1 |
| 50-year | 5.0200 | 10.9200 | 1.16 | 0.126 | 1.727 | 1.16 |

#### 2.7.3. Irregular wave tests

The irregular wave test conditions include tests in the sea state of rated, cut out, once in 50-years under wave direction of 0°, as presented in Table 9. The test purpose of the new FWAP without or with nets under irregular waves is mainly to test the key parameters of hydrodynamic performance of the platform, including the platform motions, accelerations and tower top loads under the wave environment in the target sea area.

#### 2.7.4. Combined wind and wave tests

The combined wind and wave test conditions also include tests in the sea state of rated, cut out, once in 50-years under 0° wind and wave directions, as shown in Table 10. The 0° indicates the wind wheel is facing the incoming wind direction. The wind and wave directions are always consistent, which means the wind and wave loads are always in the same direction. The test purpose of the new FWAP under combined wind and wave is mainly to test the key parameters of coupling dynamic performance of the platform, including the platform motions, accelerations and tower top loads under the combined wind and wave environment in the target sea area.

## 3. Calibrations of environmental conditions

During the experiment, the environmental conditions are firstly simulated and calibrated. The simulation of the marine environmental conditions in the water mainly includes simulation of wind, simulation of wave (simulation of white noise waves and simulation of irregular waves).

### 3.1. Wind calibrations

The simulation of the stroke field uses a 3 × 3 array axial fan system to generate constant air with effective air creation area of 3.76m × 3.76m and maximum model wind speed of 9.53 m/s (Fig. 2). To improve the quality of the wind field and increase the uniformity of the wind speed, a honeycomb fairing was installed at the front of the wind creation system, as shown in Fig. 11.

All simulations of wind in this test are constant wind, corresponding to three test conditions: rated, cut out and once in 50 years. The full-size wind speed and corresponding model test wind speed in each condition are shown in Table 10.

When simulating the test condition of the power generation state, it should be ensured that the tip speed ratio is similar, which is:

$$TSR_m = \frac{\omega_m R_m}{V_{wm}} = \frac{\omega_s R_s}{V_{ws}} = TSR_s$$

where $\omega$ is the rotational angular velocity of the rotor, $R$ denotes the radius of rotor, $V$ is the wind speed. TSR similarity can ensure that the rotor rotation speed, system excitation frequency due to rotor imbalance and the aerodynamic interaction between tower and blade are the same as those of the prototype.

From the perspective of motion similarity, the similarity of tip speed

**Table 10**
Combined wind and wave test conditions.

| Sea states | Prototype | | | | | Model | | | | |
|---|---|---|---|---|---|---|---|---|---|---|
| | wind | Wave | | | Wind turbine | wind | Wave | | | Wind turbine |
| | V (m/s) | Hs (m)\1 | Tp (s)\1 | γ | ϖ (rpm)\1 | V (m/s)\1 | Hs (m)\1 | Tp (s)\1 | γ | ϖ (rpm)\1 |
| Rated | 10.5 | 0.979 | 5.946 | 1 | 13.36 | 1.66 | 0.024 | 0.94 | 1 | 84.496 |
| Cut out | 25 | 3.442 | 7.411 | 1 | 13.36 | 3.953 | 0.086 | 1.172 | 1 | 84.496 |
| 50-year | 46.2 | 5.02 | 10.92 | 1.16 | 0 | 7.305 | 0.126 | 1.727 | 1.16 | 0 |

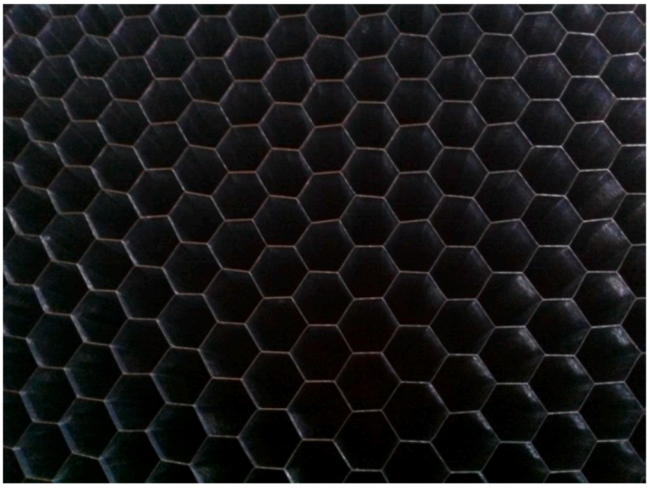

**Fig. 11.** Honeycomb fairing.

ratio (TSR) only counts for the working conditions when the wind turbine is rotating (Under 50-year wind, the wind turbine has no rotation), so only the model values of wind speed for the wind conditions of rated and cut out in Table 10 are simulated to ensure similar TSR in this test. Note that since the model value of wind speed corresponding to the wind speed is extra high under 50-year condition, the extreme wind speed in this situation is adjusted from the perspective of thrust similarity.

Wind speed calibration should be carried out before the test. The mean of the wind speed timing data measured by the thermal membrane wind speed sensor calibrated by the wind tunnel is used as a reference for the wind simulation. The layout height of the wind speed sensor and the distance to the wind making device are consistent with the corresponding position of the hub center in the formal test so that the measured data of the thermal film anemometer is consistent with the wind speed at the hub center in the formal test. After a period of acquisition, the comparison between the results of the final wind simulation and the target value under rated and cut out conditions is shown in Fig. 12 and Table 11. The accuracy of the wind simulation in working conditions of rated and cut out and the relative error of the target value are controlled within 1%, and the turbulence degree is less than 6.6%, which meets the test requirements.

Wind turbine thrust test involves thrust test under three different wind speeds including under rated, cut out and 50-year conditions. Among them, the thrust test under extreme wind speed is specially designated by wind turbine manufacturer. The test should be performed while the wind turbine is facing the wind sideways in order to simulate an extreme situation in the face of severe sea conditions and yaw failure. The wind turbine thrust test results are as follows. All results are model scales, and the deviation between the average value of thrust measurement and the target value under all working conditions is within 1%, as presented in Table 12 and Fig. 13.

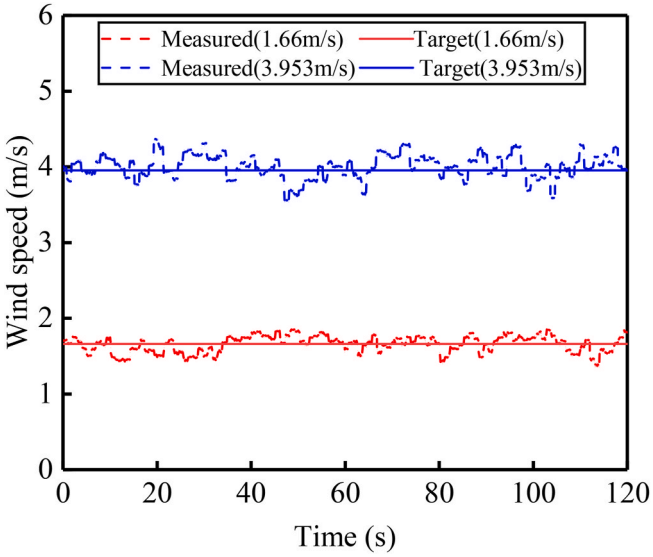


**Fig. 12.** Simulation of the rated and cut out wind speeds.

**Table 11**
The comparison of wind simulation and target values.

| Sea states | Target wind speed ( m/s ) | Mean wind speed of simulation ( m/s ) | Relative error ( - ) | Turbulence degree ( - ) |
|---|---|---|---|---|
| Rated | 1.66 | 1.658 | −0.11% | 6.55% |
| Cut out | 3.953 | 3.927 | −0.65% | 5.47% |

**Table 12**
Wind turbine thrust test results.

| Sea states | Target thrust (N) | Thrust direction | Measurements (N) | Deviation |
|---|---|---|---|---|
| Rated | 11.131 | Front | 11.084 | −0.42% |
| Cut out | 3.445 | Front | 3.466 | 0.61% |
| Extreme | 4.567 | Sideway | 4.584 | 0.39% |

### 3.2. Wave calibrations

In the test, the waves required to undergo environmental calibration include four irregular waves (including one white noise wave). The parameters of the environmental conditions required simulated and their corresponding model values are listed in Tables 8–10.

Irregular waves in the pools are simulated according to the given spectrum, significant wave height, and spectral peak period. Two-parameter JONSWAP spectra are used for the waves. The target spectrum formula is given as follows:

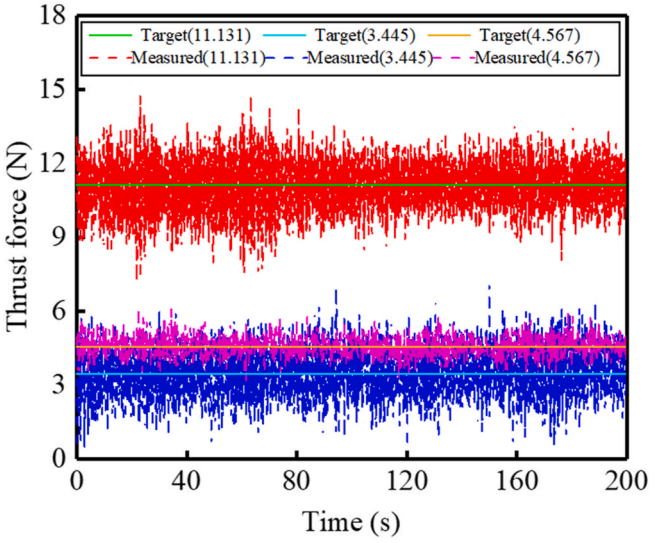


**Fig. 13.** Wind turbine thrust measurement results under rated, cut out and 50-year conditions.

$$S(f) = \alpha H_S^2 T_p^{-4} f^5 \exp\left[-1.25\left(T_p f\right)^{-4}\right] \gamma^{\exp\left[-\frac{(T_p f-1)^2}{2\sigma^2}\right]}$$

where $S(f)$ is spectral density, $f$ and $H_S$ represent frequency of wave and significant wave height, $T_p$ denotes period of spectral peak, $\gamma$ and $\sigma$ are parameters.

The comparison of the wave spectrum analysis results obtained from the measurement of wave simulation in the wave-only conditions of rated, cut out, once in 50 years and white noise wave and the target spectrum parameters are demonstrated in Fig. 14 respectively. As seen from Fig. 14, the significant wave heights and periods of spectral peak of the simulated waves in the test all meet the accuracy requirements that the error is less than 5% [35,36].

## 4. Experimental results

### 4.1. Still water decay tests

The free decay test results of the new FWAP without or with nets are shown in Fig. 15. In general, the decay test results are as expected, except sway. In the sway decay test, the sway motion is highly coupled with roll and yaw motion, and the expected sway-only decay cannot be obtained. The reason for this phenomenon is mainly due to the asymmetry of the mooring system in the sway direction.

Comparing the results without and with nets, it is found that the nets have an influence on the decay results of the system. The main effect is reflected in the damping of the system. It can be observed from Fig. 15 that the existence of nets significantly improves the damping of the system. In addition, the motion periods are increased while nets are included. As shown in Fig. 15, the natural periods of heave, pitch and roll for the FWAP without and with nets are almost the same in free-floating state. In the moored state, the measured natural periods of all motions with nets are obviously larger than those without nets, especially for sway and yaw. The increase of natural periods can be attributed to the change of system damping when nets are included.

### 4.2. White noise wave tests

In this model test, the white noise wave test is divided into two categories: with and without nets, and the wave incidence angle is 0°. The RAOs of the FWAP without or with nets obtained in the experiment are shown in Fig. 16.

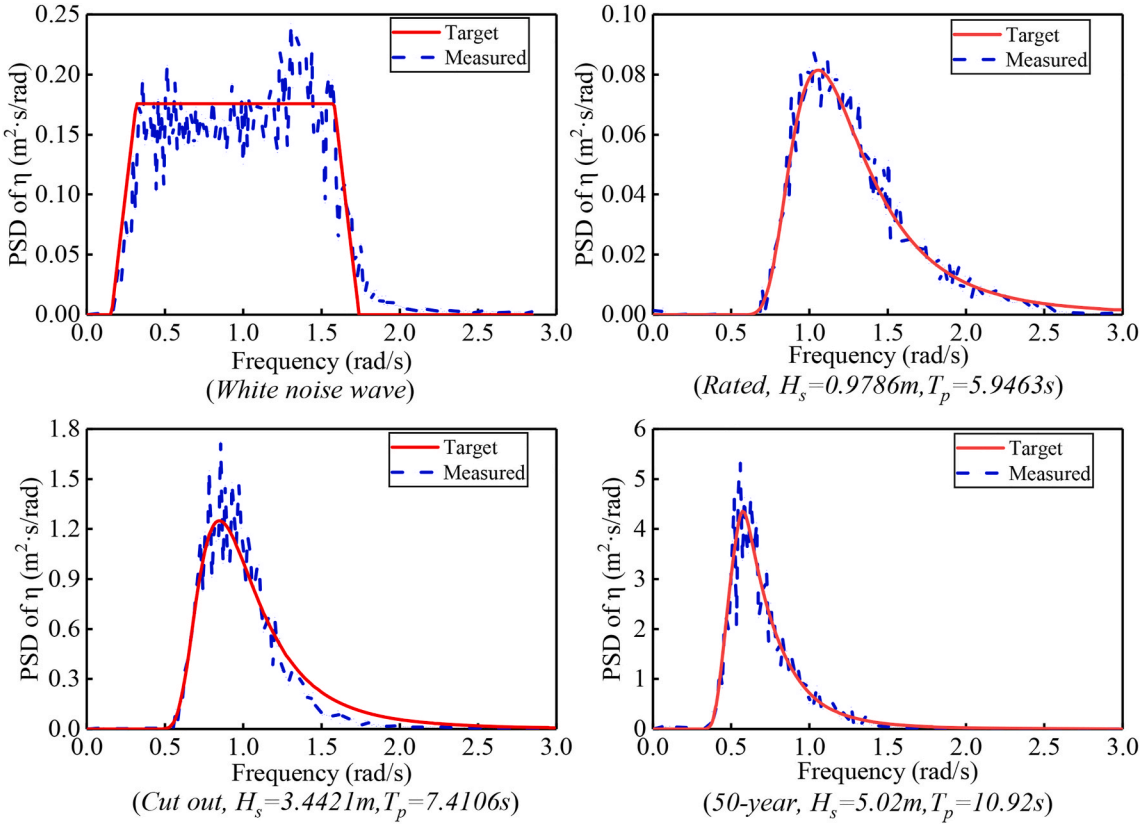


**Fig. 14.** The comparison of wave spectrum analysis results and target spectrum.

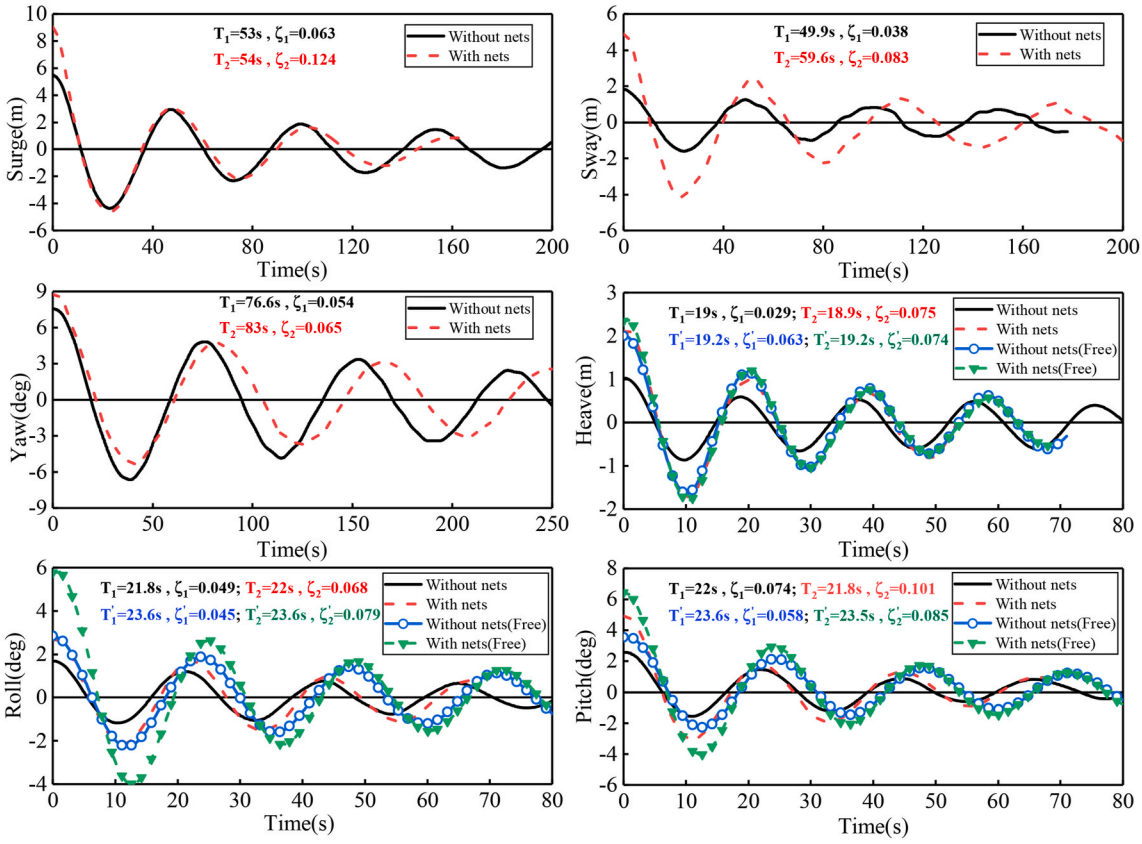


**Fig. 15.** Still water decay test results.

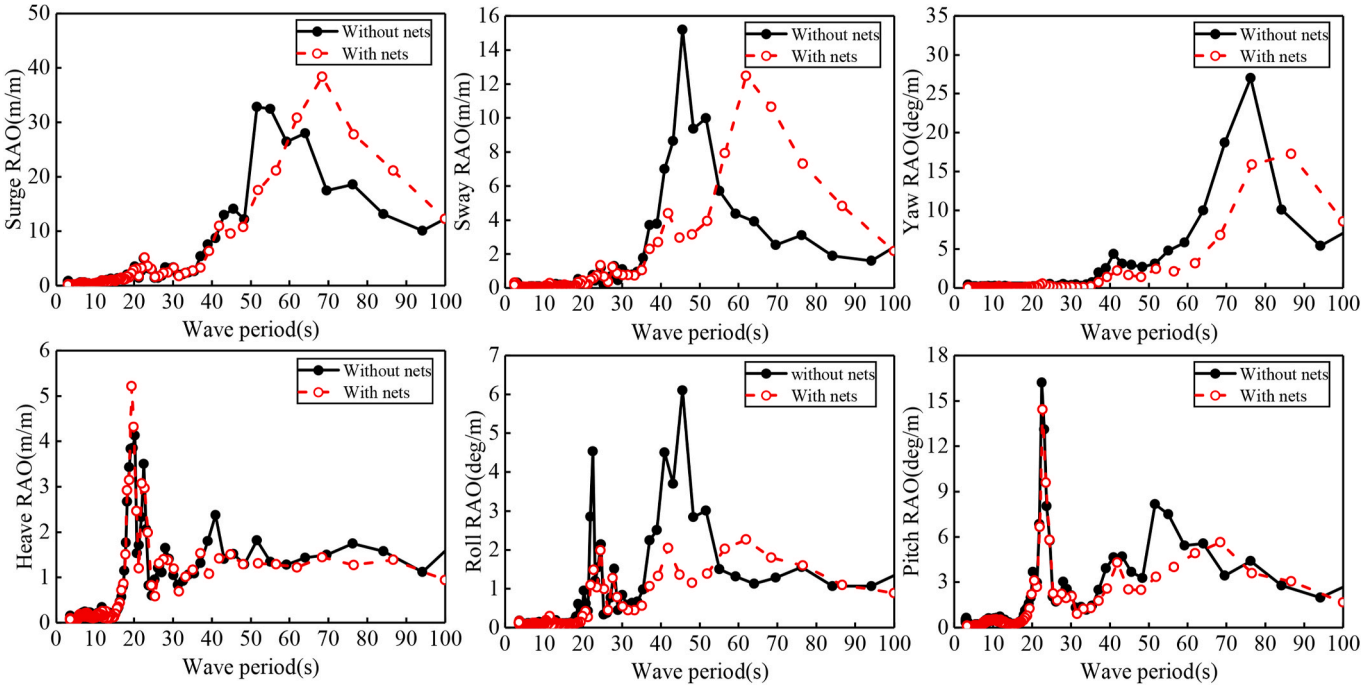


**Fig. 16.** White noise wave test results.

Clearly, RAOs of surge, sway and yaw motions firstly increase and then decrease with the increase of wave periods for the new FWAP without or with nets. Note that RAOs of surge, sway and yaw without nets are larger than those with nets when the wave periods are small. This is because the damping due to the existence of nets has a notable effect on surge and sway response. As a result, RAOs of the FWAP with nets are lower compared with those without nets. While wave periods continue to increase, RAOs of surge, sway and yaw for FWAP with nets

keep increasing with the appearance of maximum values later than those without nets. This can be explained by that the damping effect induced by nets is weakened with the increase of wave periods, wherein the wave load plays a dominated role for the new FWAP with nets. Consequently, RAOs of surge, sway and yaw for the new FWAP with nets are larger than those without nets when wave periods are large.

As for heave, roll and pitch response, RAO values for the new FWAP without or with nets are almost the same when wave periods are small, indicating that the damping due to nets scarcely have an effect on these motions. With the increase of wave periods, the damping effect induced by nets can be obviously observed, as shown in Fig. 16. However, RAOs of heave, roll and pitch with nets are clearly smaller than those without nets at around wave period of 50s–60s, which can be attributed to the damping effect of nets. As wave periods keeps increasing, the damping effect induced by nets decreased, resulting in almost same RAOs of heave, roll and pitch response under larger wave periods.

### 4.3. Irregular wave tests

#### 4.3.1. Motion responses

The main motions of the new FWAP without or with nets are selected to analyze and discuss here, namely, the surge motion, heave motion and pitch motion. Correspondingly, the maximum, minimum, mean and standard deviation values of the motion of the new FWAP under the sea state rated, cut out, once in 50 years are presented in Figs. 17–19. The height of the rectangular boxes in the box charts is twice the standard deviation (STD). In this way, the meaningful values of the response for the new FWAP without or with nets are presented.

It can be seen that under rated sea state, the maximum surge amplitude of the new FWAP without nets is about 0.700 m, which is much smaller compared with those under cut out and 50-year extreme sea states. The maximum distance of surge can be up to around 4.00 m and 4.094 m under the latter two sea states. Likewise, the maximum values of heave and pitch motions also show a similar changing trend while the new FWAP without nets are under these three different sea states. As shown in Figs. 18 and 19, the maximum amplitude of heave motion is 0.743 m, 1.156 m and 1.411 m respectively under rated, cut out and 50-year extreme sea states while the maximum pitch motions of 0.501°, 1.574° and 3.131° can be detected. The increasing trend of these three motion amplitudes can be attributed to the enlarged wave loads when the sea state is changed. As the wave height is increased, more energy is included inside, leading to larger wave loads when interacting with the new FWAP. Consequently, larger motion amplitudes can be observed for the new FWAP without nets under cut out and 50-year extreme sea states.

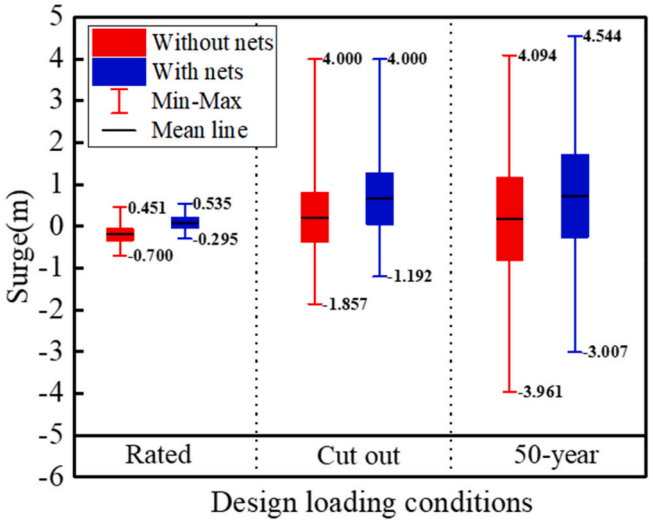


**Fig. 17.** Surge response of the new FWAP under only irregular wave.

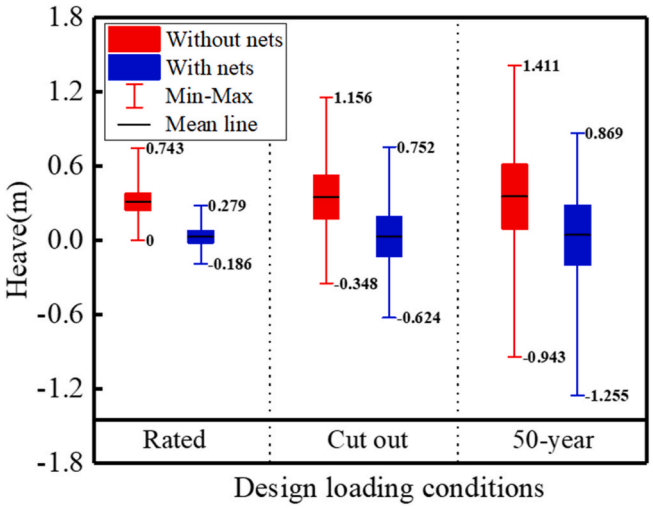


**Fig. 18.** Heave response of the new FWAP under only irregular wave.

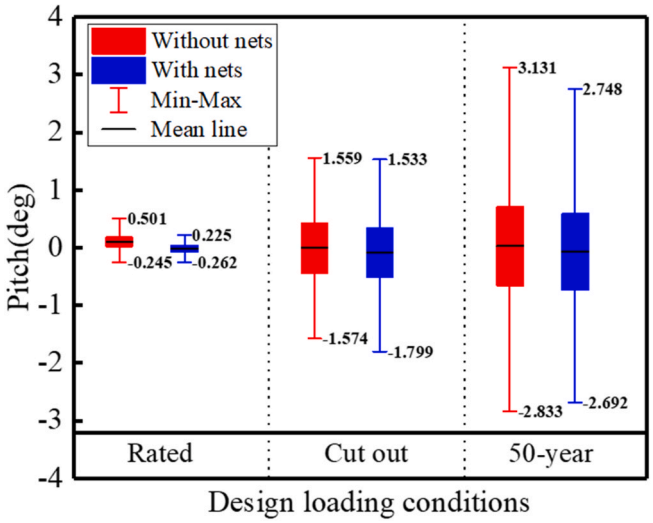


**Fig. 19.** Pitch response of the new FWAP under only irregular wave.

While the nets are included for the new FWAP, the maximum amplitudes of surge, heave and pitch are also amplified when the platform undergoes rated, cut out and 50-year extreme sea states in sequence, as observed in Figs. 17–19. For instance, the maximum surge and heave amplitudes are 0.535 m and 0.279 m respectively under rated sea state. As the FWAP is subjected to wave loads of 50-year extreme sea state, the maximum amplitudes of surge and heave are increased up to about 4.544 m and 1.255 m respectively. Moreover, the maximum pitch value is also increased from 0.262° to 2.748° when the environmental condition changes from rated to 50-year extreme sea state. Such change of motion amplitude can also be explained by that larger wave loads are exerted on the new FWAP with nets under 50-year extreme sea state.

As for the effect of nets on motions of the new FWAP, it can be found that the maximum amplitudes of motions are decreased compared with those without nets under all three sea states. When the nets are taken into account, the maximum values of surge are reduced from 0.700 m, 4.00 m and 4.094 m to 0.535 m, 4.00 m and 4.544 m respectively under rated, cut out and 50-year extreme sea states. Similarly, the amplitudes of heave and pitch motions are also decreased compared with those without nets under each sea state, as observed in Figs. 17 and 18. Such reduction of all the motion amplitudes can be explained by the damping

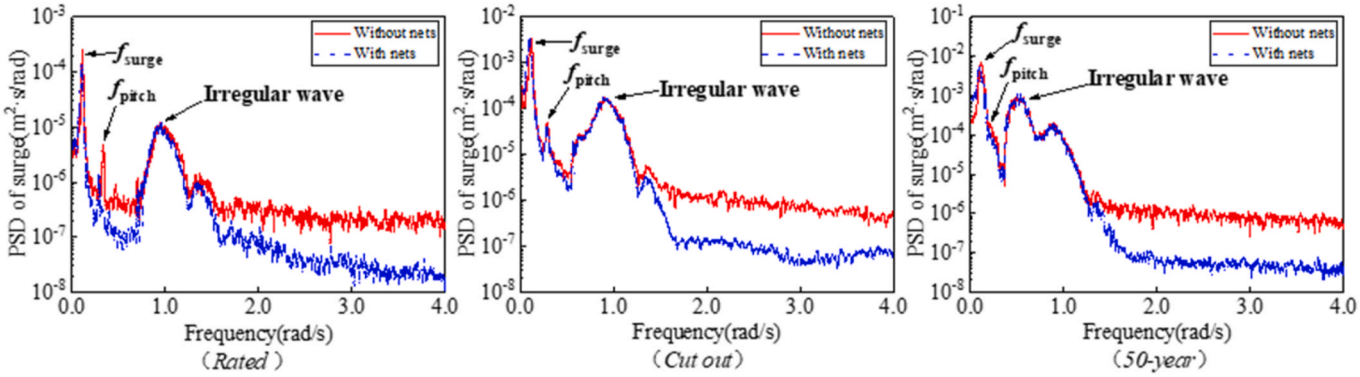


**Fig. 20.** Power spectra of surge response of the new FWAP under only irregular wave.

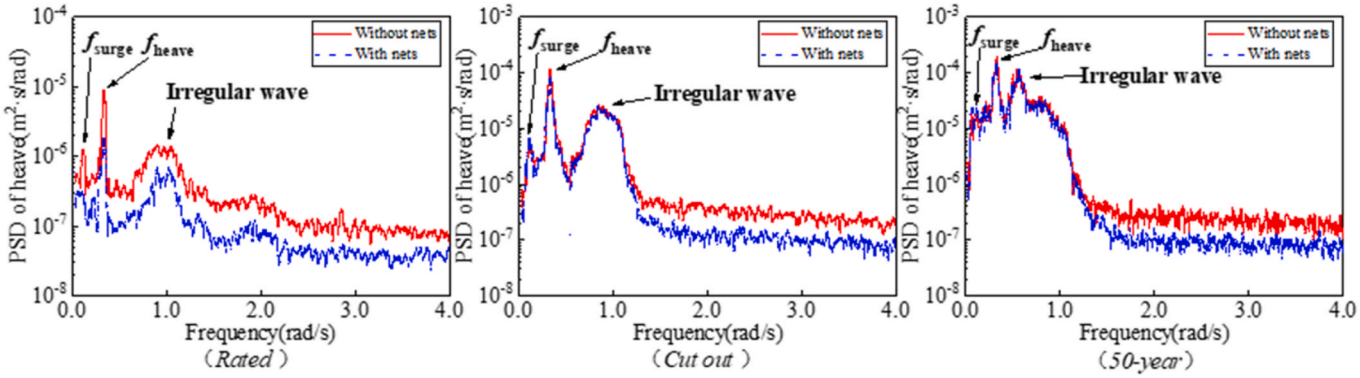


**Fig. 21.** Power spectra of heave response of the new FWAP under only irregular wave.

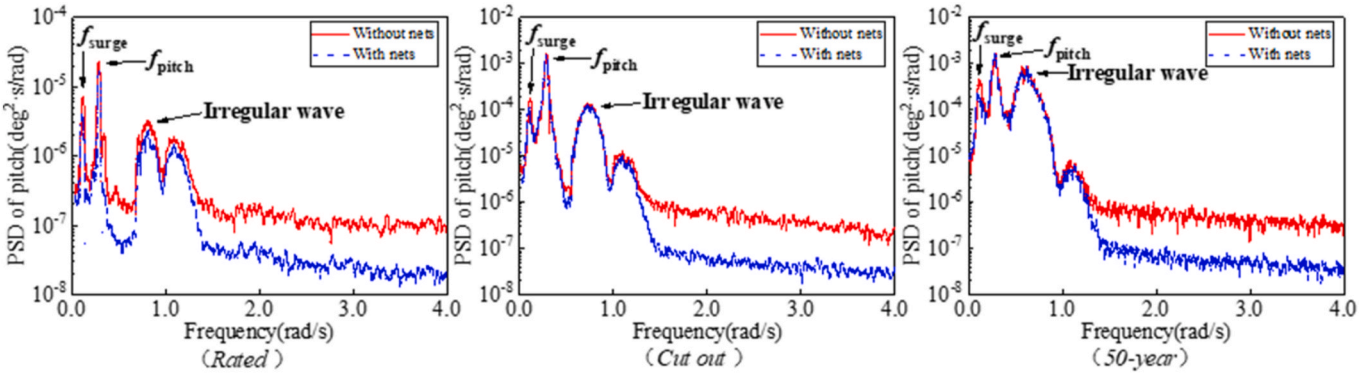


**Fig. 22.** Power spectra of pitch response of the new FWAP under only irregular wave.

effect caused by the existence of nets.

The power spectra of dynamic responses of the new FWAP under rated, cut out and 50-year extreme sea states are also demonstrated in Figs. 20–22. It can be seen that multi power components are included for the motion response of the new FWAP regardless of nets. Due to the coupling of surge and pitch motions, there exist power peaks $f_{surge}$ and $f_{pitch}$ corresponding to these two motions under different sea states, as shown in Fig. 20. The frequency of around 0.12 rad/s and 0.29 rad/s corresponding to surge and pitch response can be detected under these three sea states, especially for rated and cut out sea states. In terms of heave motion, frequency peak $f_{heave}$ of 0.33 rad/s is also captured with coupling frequency 0.12 rad/s of surge motion (Fig. 21). Besides, there exist evident power peaks $f_{ir}$ accordant to irregular waves. When the marine environmental condition changes from rated to 50-year extreme sea state, the dominance of irregular waves is strengthened while the coupling between responses are weakened. The predominated effect of irregular wave under 50-year extreme sea state can be ascribed to the enlarged wave load on the new FWAP under this circumstance.

It can be also evidently found that nets can exert little effect on the power spectra of surge, heave and pitch motions of the new FWAP. When nets are integrated with the offshore wind turbine, the power spectra are scarcely changed compared with those without nets. Noteworthy is that more energy can be allocated on high-frequency component due to the presence of nets.

### 4.3.2. *Platform accelerations*

The statistical maximum values of the longitudinal, lateral and vertical accelerations of the new FWAP under rated, cut out and 50-year extreme sea state are illustrated in Figs. 23–25. For the new FWAP without or with nets, the maximum values of platform accelerations in

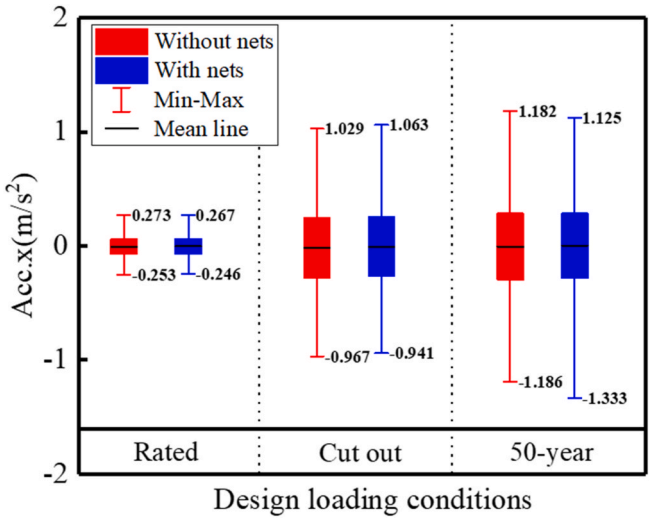


**Fig. 23.** Longitudinal accelerations of the new FWAP under only irregular wave.

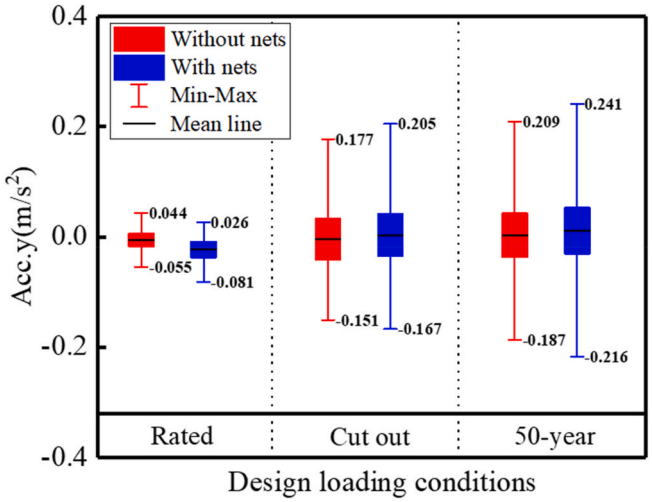


**Fig. 24.** Lateral accelerations of the new FWAP under only irregular wave.

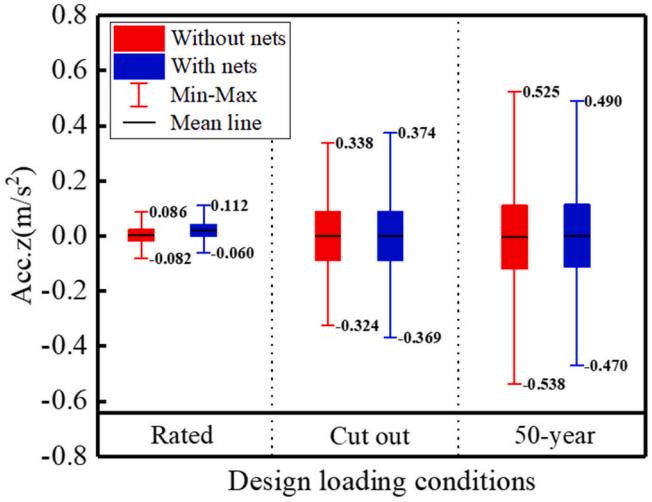


**Fig. 25.** Vertical accelerations of the new FWAP under only irregular wave.

longitudinal, lateral and vertical directions under only irregular wave are increased when the oceanic condition changes from rated to 50-year extreme sea state. As shown in Fig. 23, under rated sea sate, the maximum accelerations are 0.273 m/s$^2$, 0.055 m/s$^2$ and 0.086 m/s$^2$ in longitudinal, lateral and vertical directions for the FWAP without nets while those with nets of 0.267 m/s$^2$, 0.081 m/s$^2$ and 0.112 m/s$^2$ can be detected. When the new FWAP undergoes 50-year extreme sea state, the maximum longitudinal acceleration Acc.x, lateral acceleration Acc.y and vertical acceleration Acc.z without nets are increased up to 1.186 m/s$^2$, 0.209 m/s$^2$ and 0.538 m/s$^2$ while those with nets are up to 1.333 m/s$^2$, 0.241 m/s$^2$ and 0.490 m/s$^2$. The increase of accelerations can be explained by that the wave load exerted on the new FWAP without or with nets under 50-year extreme sea state is much larger than that under rated sea state, leading to larger accelerations.

It should be noticed that the influence of nets on the accelerations is not notable. It can be seen from Figs. 23–25 that under three sea states, the maximum longitudinal acceleration Acc.x, lateral acceleration Acc.y and vertical acceleration Acc.z of the new FWAP with nets are not changed evidently compared to those without nets. For instance, under rated sea state, the maximum accelerations of 0.273 m/s$^2$, 0.055 m/s$^2$ and 0.086 m/s$^2$ in longitudinal, lateral and vertical directions are captured for the FWAP without nets respectively. With the presence of nets, the maximum values of Acc.x, Acc.y and Acc.z are changed to 0.267 m/s$^2$, 0.081 m/s$^2$ and 0.112 m/s$^2$, indicating that the nets have a limited effect on the acceleration of the new FWAP exposed to only irregular wave.

The power spectra of accelerations of the new FWAP in longitudinal, lateral and vertical directions under rated, cut out and 50-year extreme sea states are demonstrated in Figs. 26–28. For the longitudinal acceleration Acc.x and lateral acceleration Acc.y with or without nets, the influence of surge can be evidently observed, which is presented by the frequency peak of 0.12 rad/s. But the vertical acceleration Acc.z is not affected by surge motion, as shown in Fig. 28. Besides, the frequency peaks of 0.33 rad/s and 0.29 rad/s corresponding to heave and pitch are also detected for Acc.x and Acc.z while the ones with values of 0.12 rad/s and 0.29 rad/s induced by sway and roll can be observed in Fig. 27. Moreover, since the tower top vibration is excited, the first-mode tower vibration frequency $f_{FA}^1$ of 3.45 rad/s in fore-aft direction is captured for Acc.x and Acc.z while $f_{SS}^1$ with value of 3.39 rad/s in side-side direction appears for Acc.y. Noteworthy is that the frequency peaks induced by irregular wave always play a dominated role among all the power spectra under rated, cut out and 50-year extreme sea states. The frequency peak of $f_{SS}^1$ is weakened for Acc.y when the environmental condition changes from rated to 50-year extreme sea state. Nonetheless, $f_{FA}^1$ is scarcely influenced by sea states, as shown in Figs. 26 and 28. As for the effect of nets, the presence of nets exerts little effect on power spectra of Acc.x, Acc.y and Acc.z.

### 4.3.3. *Tower top loads*

The typical tower top loads of the new FWAP without or with nets under rated, cut out and 50-year extreme sea state are displayed in Figs. 29–31. Likewise, the maximum values of longitudinal tower top load $F_x$ and lateral tower top load $F_y$ as well as horizontal bending moment $M_y$ of the new FWAP without or with nets are also changed under rated, cut out and 50-year extreme sea states. As shown in Figs. 29 and 30, regardless of nets, the maximum values of $F_x$ and $F_y$ under rated sea states are much lower than those under cut out and 50-year extreme sea states. In terms of $M_y$, similar changing trend is also observed under different sea states. For instance, under rated sea state, the maximum values of $F_x$ and $F_y$ of the new FWAP without nets are 124 kN and 26.66 kN while those with nets are 112.2 kN and 23.03 kN respectively. Moreover, the maximum $M_y$ without or with nets are 202.3 kN•m and 167.8 kN•m respectively. As the FWAP undergoes wave loads under 50-year extreme sea state, the maximum values of $F_x$ and $F_y$ as well as $M_y$ are increased dramatically, regardless of nets. It can be seen that the

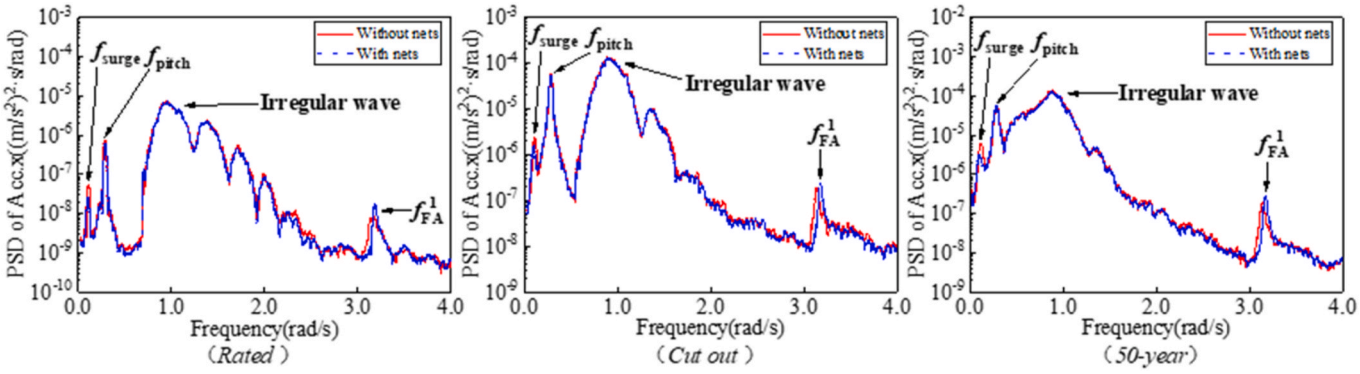


**Fig. 26.** Power spectra of longitudinal accelerations of the new FWAP under only irregular wave.

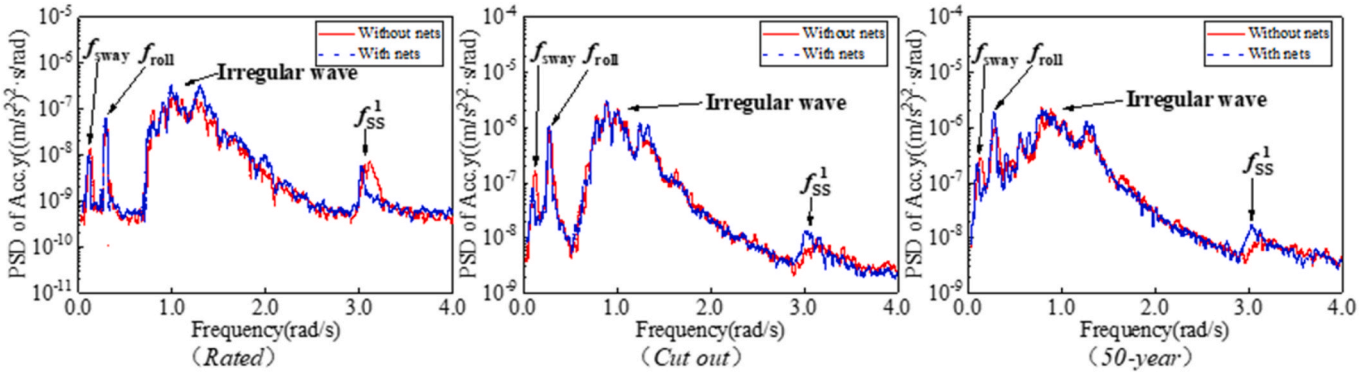


**Fig. 27.** Power spectra of lateral accelerations of the new FWAP under only irregular wave.

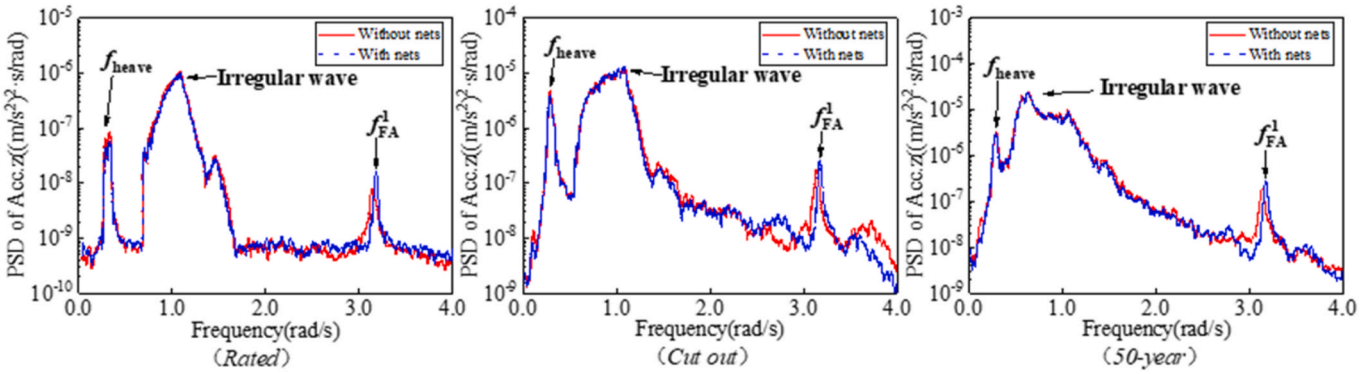


**Fig. 28.** Power spectra of vertical accelerations of the new FWAP under only irregular wave.

maximum $F_x$ and $F_y$ of 681.7 kN and 90.28 kN can be detected for the new FWAP without nets. Meanwhile, the maximum value of horizontal bending moment is increased up to 1416 kN•m. When the nets are included, the maximum values of $F_x$, $F_y$ and $M_y$ are also up to 599.8 kN, 84.83 kN and 934.9 kN•m under 50-year extreme sea state. The increase of $F_x$ and $F_y$ as well as $M_y$ without or with nets can be attributed to the enlarged wave loads exerted on the FWAP under different sea states.

It can also be observed that the existence of nets has an effect on the longitudinal tower top load $F_x$ and lateral tower top load $F_y$, particularly for the horizontal bending moment $M_y$ of the new FWAP. Moreover, the decrease is notable under 50-year extreme sea state. As seen in Figs. 29 and 30 and 31, the maximum values of $F_x$ and $F_y$ as well as $M_y$ with nets are almost same as those without nets under rated sea state. When the FWAP without nets is under 50-year extreme sea sates, $F_x$, $F_y$ and $M_y$ with maximum values of 681.7 kN, 90.28 kN and 1416 kN•m are detected. But the maximum values of these tower top loads are decreased to 599.8 kN, 84.83 kN and 934.9 kN•m due to the damping effect of nets.

The power spectra of the longitudinal tower top load $F_x$ and lateral tower top load $F_y$ as well as the horizontal bending moment $M_y$ of the new FWAP without or with nets are also depicted in Figs. 32–34. Obviously, multi frequency response can be detected for $F_x$, $F_y$ and $M_y$ for the new FWAP with or without nets under rated, cut out and 50-year extreme sea states. Due to the motion of surge and pitch, frequency peaks of 0.12 rad/s and 0.29 rad/s appear for $F_x$ and $M_y$. In addition, sway and roll also exert an effect on the tower loads, which can be represented by the frequency peaks of 0.12 rad/s and 0.29 rad/s on $F_y$. Similar to the power spectra of motion and acceleration, pretty wide frequency bandwidth induced by irregular wave can be captured, proving the dominant effect of irregular wave on the tower top loads.

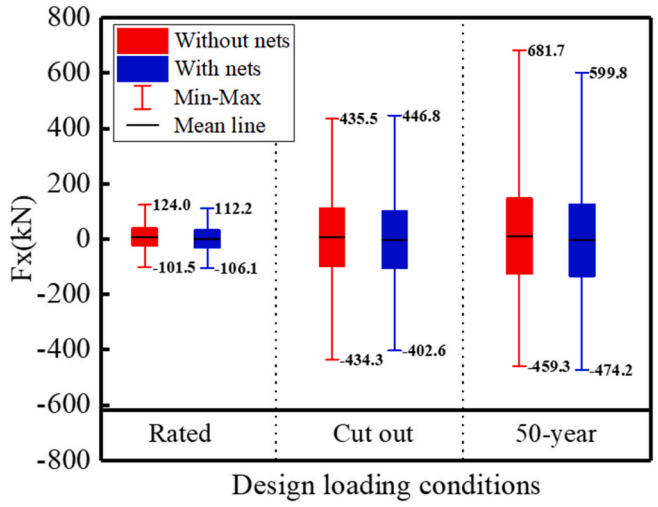


**Fig. 29.** Longitudinal tower top loads of the new FWAP under only irregular wave.

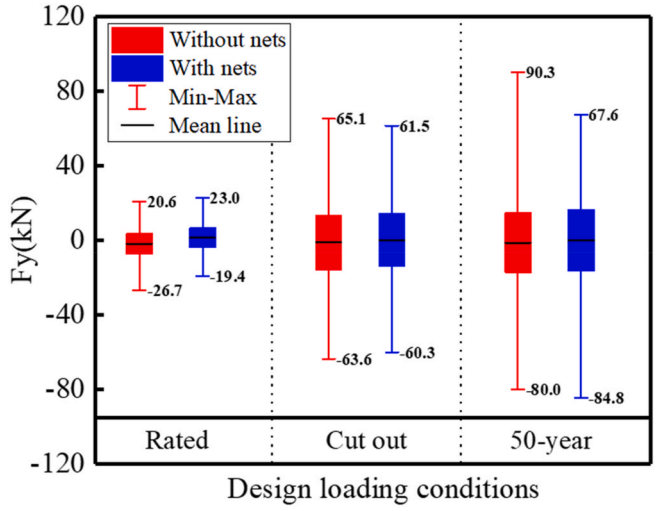


**Fig. 30.** Lateral tower top loads of the new FWAP under only irregular wave.

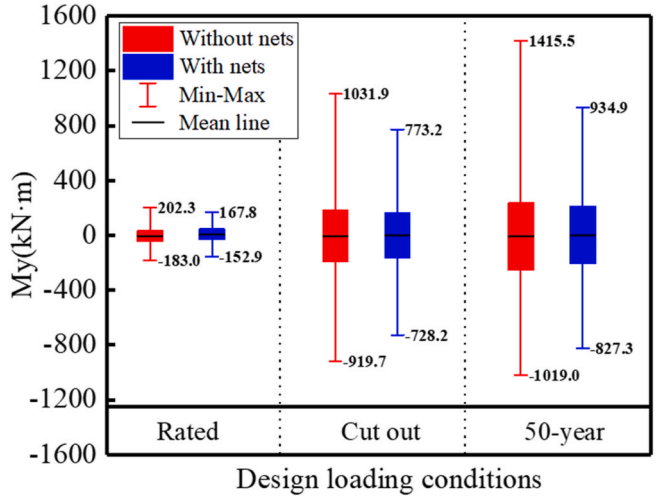


**Fig. 31.** Horizontal bending moments of the new FWAP under only irregular wave.

Moreover, the excitation of first mode tower vibration in fore-aft direction results in the existence of $f_{FA}^{1}$ 3.45 rad/s for $F_x$ and $M_y$. In terms of $F_y$, $f_{SS}^{1}$ of 3.39 rad/s can be detected due to the occurrence of first mode tower vibration in side-side direction. When the nets are considered for the new FWAP, the power spectra of $F_x$, $F_y$ and $M_y$ are seldom changed, indicating that the effect of nets is very limited on the tower top loads.

### 4.4. Wind and wave test results

#### 4.4.1. Motion responses

The characteristics of the surge, heave and pitch motions of the new FWAP without or with nets undergoing combined wind and wave are shown in Figs. 35–37. Similar to the response under only irregular wave, regardless of nets, the maximum surge, heave and pitch of the new FWAP are small under rated sea state while their maximum values are notably increased under cut out and 50-year extreme sea states. As is shown in Fig. 35, the maximum horizontal drift distance of the new FWAP is about 3.162 m without nets and 3.292 m with nets. When the FWAP undergoes 50-year extreme sea state, the platform moves with maximum surge of 6.159 m without nets and 6.322 m with nets. Without nets, the maximum amplitudes of heave and pitch are 0.306 m and 1.302° respectively while those values with nets are 0.306 m and 1.220° under rated sea state. When the oceanic condition changes to 50-year extreme sea state, the maximum values of heave and pitch without nets are increased up to 1.350 m and 3.507° while those with nets are also up to 1.084 m and 3.310°, as seen in Fig. 37. The reason for the increase of the motion amplitude can be attributed to the enlarged wave loads exerted on the FWAP while the sea state is changed. Although wind can exert an impact on the motion of the new FWAP, the changing trend of motion under different sea states is still predominantly affected by wave loads.

Noteworthy is that the existence of the nets exerts an excitation effect on surge motion while the damping effect induced by nets can be evidently observed for heave and pitch responses. Under rated, cut out and 50-year extreme sea states, the maximum surge amplitudes with nets are amplified compared to those without nets, indicating that nets can intensify surge response. As seen in Fig. 35, the new FWAP without nets moves with the maximum surge values of 3.162 m and 6.159 m under rated and 50-year extreme sea states respectively. When nets are included, the maximum surge values are increased to 3.297 m and 6.332 m. Nevertheless, the maximum amplitudes of heave and pitch are reduced due to the damping effect incurred by nets. For example, the maximum heave and pitch values of 1.350 m and 3.507° are observed under 50-year extreme sea state. But the presence of nets decreases these two maximum amplitudes to 1.084 m and 3.310°, which proves the damping influence caused by nets.

The power spectra of surge, heave and pitch under rated, cut out and 50-year extreme sea states are presented in Figs. 38–40. It is also obvious that there exist multi power spectra for all the motions of the new FWAP without or with nets, including the ones corresponding to each motion and irregular wave. Similar as those under only irregular wave, wide frequency bandwidth induced by irregular wave can be observed under all three sea states. And frequency of 0.12 rad/s for surge, 0.33 rad/s for heave and 0.29 rad/s for pitch can be detected, as shown in Figs. 38–40. In addition, the coupling of motions can also be observed in the power spectra of motions, proving the interaction between motions.

In addition, there exist wind turbine 1P, 2P and 3P excitations for the motion due to the rotation of the wind turbine, especially for the power spectra of heave and pitch. This phenomenon is also observed in the work of Lei et al. [30]. The frequency peaks of wind turbine 1P, 2P and 3P excitations can be evidently observed for heave and pitch under rated sea state, but not for surge, indicating the notable effect of wind turbine on heave and pitch. As the marine environmental condition changes to cut out sea state, the occurrence of 1P, 2P and 3P excitations can still be detected for heave and pitch. But the power spectra corresponding to 1P,

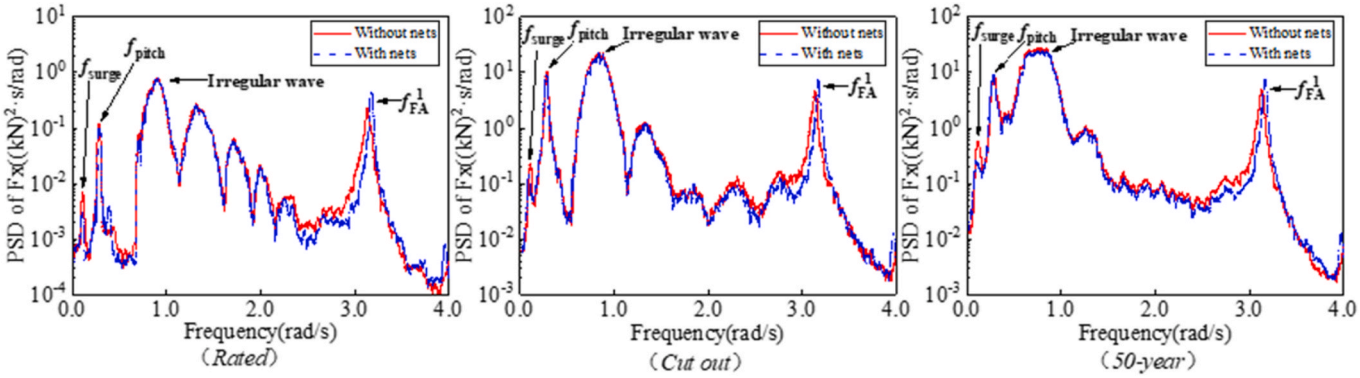


**Fig. 32.** Power spectra of longitudinal tower top loads of the new FWAP under only irregular wave.

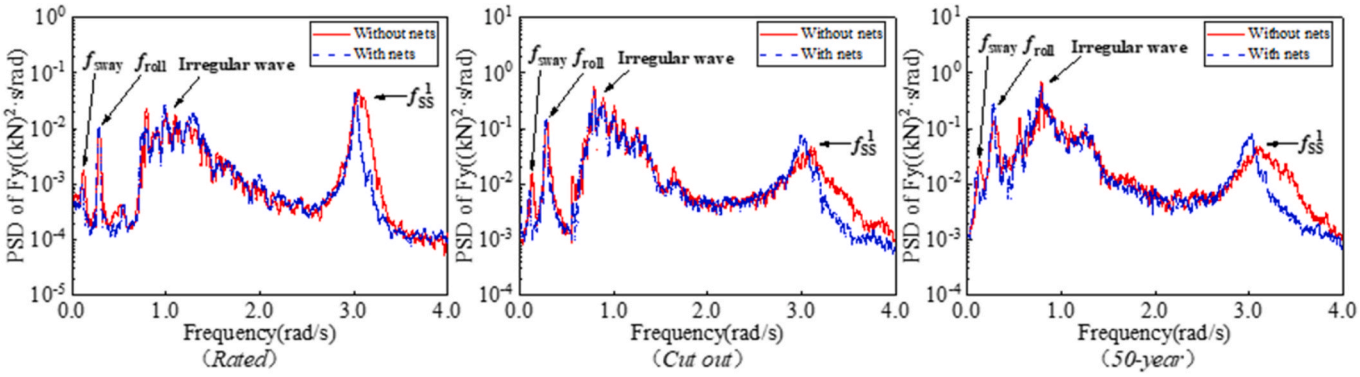


**Fig. 33.** Power spectra of lateral tower top loads of the new FWAP under only irregular wave.

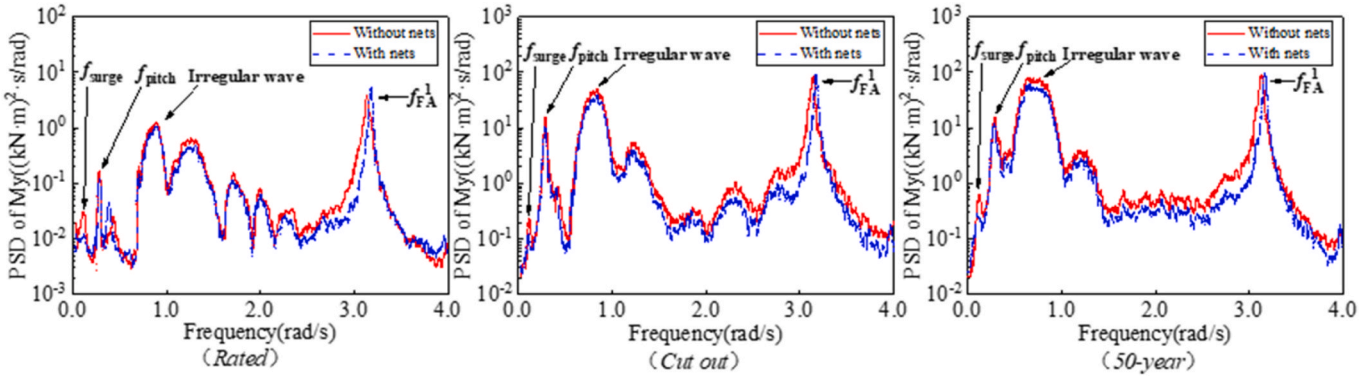


**Fig. 34.** Power spectra of horizontal bending moments of the new FWAP under only irregular wave.

2P and 3P excitations are weakened. When the new FWAP without or with nets undergoes 50-year extreme sea state, 1P, 2P and 3P excitations disappear for all the motions, which can be attributed to nonrotation of wind turbine under this circumstance.

It can be also seen that the energy allocation on the power spectra of motions is affected by the existence of nets, as shown in Figs. 38–40. Clearly, nets have little effect on the component of low frequency motions. Nonetheless, with the presence of nets, more energy is allocated on the high frequency components of motions.

### 4.4.2. Platform accelerations

The accelerations of the new FWAP without or with nets under combined wind and wave are demonstrated in Figs. 41–43. As observed in Figs. 41 and 43, the longitudinal acceleration Acc.x and the vertical acceleration Acc.z of the new FWAP without or with nets show a similar changing trend while the oceanic condition is changed from rated to 50-year extreme sea state. Under rated sea state, the maximum values of Acc.x and Acc.z without nets are 0.444 m/s$^2$ and 0.241 m/s$^2$ while the maximum values of 0.473 m/s$^2$ and 0.248 m/s$^2$ are detected for those with nets. As the new FWAP is subjected to 50-year extreme sea state, the maximum amplitudes of Acc.x and Acc.z are changed to 1.261 m/s$^2$ and 0.557 m/s$^2$ without nets as well as 1.314 m/s$^2$ and 0.479 m/s$^2$ with nets. This phenomenon can be ascribed to the enlargement of thrust force due to the combined wind and wave load. When the environment condition changes from rated to cut out sea state, the thrust force exerted on the wind turbine due to wind becomes larger, leading to the increase of maximum Acc.x and Acc.z. Nevertheless, when the new FWAP is under 50-year extreme sea state, no rotation of wind turbine exists, resulting in the decrease of thrust force caused by wind. But the wave loads are remarkably increased under this circumstance compared

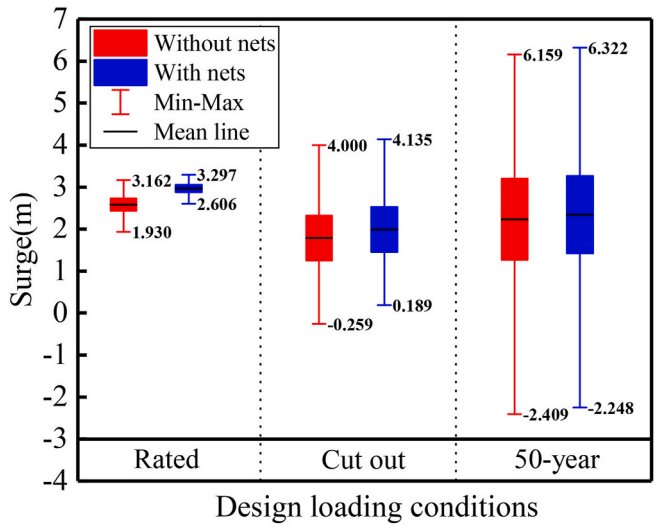


**Fig. 35.** Surge response of the new FWAP under combined wind and wave.

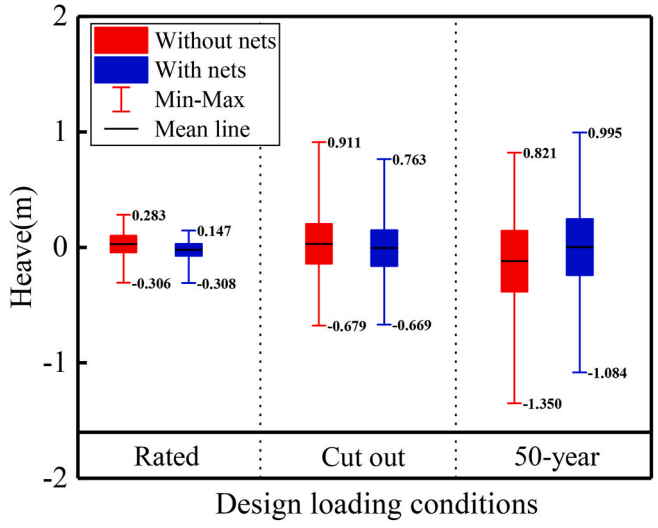


**Fig. 36.** Heave response of the new FWAP under combined wind and wave.

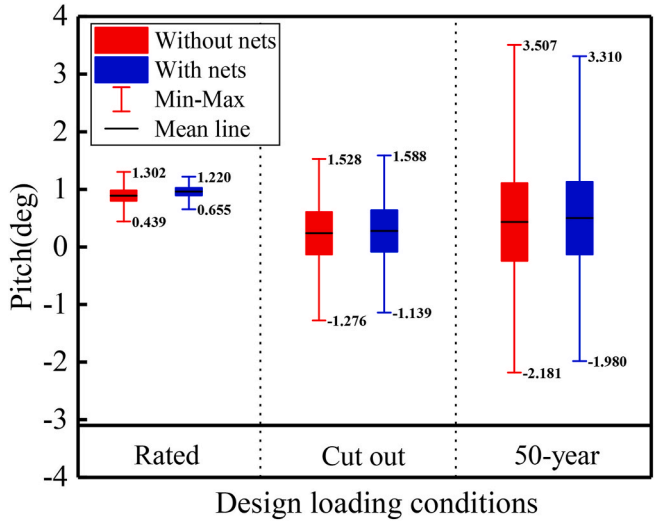


**Fig. 37.** Pitch response of the new FWAP under combined wind and wave.

with those under rated and cut out sea states. As a consequence, the maximum values of Acc.x and Acc.z still keep increasing while the new FWAP undergoes 50-year extreme sea state.

Unlike Acc.x and Acc.z, the lateral acceleration Acc.y is firstly increased and then decreased under rated, cut out and 50-year extreme sea states. As seen in Fig. 42, the maximum values of Acc.y without and with nets are equal to 0.251 m/s$^2$ and 0.227 m/s$^2$ under rated sea stated. The maximum values of 0.442 m/s$^2$ and 0.288 m/s$^2$ are observed for Acc.y without and with nets under cut out sea state. However, the maximum Acc.y without and with nets decreases to 0.221 m/s$^2$ and 0.232 m/s$^2$, when the new FWAP undergoes 50-year extreme sea state. The increase of Acc.y without and with nets under rated and cut out sea states can also be explained by the enlargement of thrust force by wind. As the oceanic condition changes to 50-year extreme sea state, the rotation of the rotor is forbidden, causing that the thrust force on the new FWAP is dramatically reduced. In addition, wave load is mainly exerted on the new FWAP in X-axis direction. As a result, the combined effect of wind and wave on Acc.y without or with nets is weakened, leading to the decrease of maximum Acc.y.

Moreover, the existence of nets has a damping effect on Acc.y, but an excitation impact on Acc.x and Acc.z under rated, cut out and 50-year extreme sea states. It can be seen from Figs. 41–43 that the maximum values of Acc.y with nets decreases compared with those without nets under three sea states. But the maximum amplitudes of Acc.x and Acc.z of the new FWAP are enlarged when nets are included. Therefore, it can be concluded that the presence of nets can act as an excitation or damping role in affecting the accelerations of the new FWAP.

The power spectra of the new FWAP accelerations without or with nets in longitudinal, lateral and vertical directions are analyzed and illustrated in Figs. 44–46. Likewise, multi power spectra corresponding to motions, irregular wave, tower vibration and rotation of wind turbine can be captured in our model test. It can be seen that Acc.x, Acc.y and Acc.z can be affected by motions of the new FWAP. There exist frequency peaks of 0.12 rad/s and 0.29 rad/s accordant to surge and pitch for Acc.x as well as the ones of 0.12 rad/s and 0.29 rad/s corresponding to sway and roll for Acc.y while the frequency of 0.33 rad/s incurred by heave is found in the power spectra of Acc.z under rated, cut out and 50-year extreme sea states, as shown in Figs. 44–46. In addition to the power spectra caused by irregular wave, the first mode tower vibrations $f_{FA}^1$ and $f_{SS}^1$ are also detected for the accelerations of the new FWAP. As presented in Figs. 44 and 45 and 46, the fore-aft frequency $f_{FA}^1$ is mainly included in the power spectra of Acc.x and Acc.z while the side-side frequency $f_{SS}^1$ is found for Acc.y under three sea states. Moreover, due to the rotation of wind turbine, the frequency peaks corresponding to wind turbine 1P, 2P and 3P excitations occur for the accelerations of the new FWAP without or with nets under rated and cut out sea states. When the oceanic condition is changed to 50-year extreme sea state, non-rotation of wind turbine results in the disappearance of 1P, 2P and 3P excitations for the power spectra of Acc.x, Acc.y and Acc.z. The existence of nets has little effect on the frequencies of Acc.x, Acc.y and Acc.z. It can also be seen from the power spectra that the wide bandwidth induced by irregular wave can be captured, while the effects of 1P, 2P, and 3P excitations of wind turbines appear as narrow-band spectra.

### 4.4.3. *Tower top loads*

The tower top loads of the new FWAP without or with nets under combined wind and wave are also examined, as demonstrated in Figs. 47–49. It can be clearly observed that the maximum values of longitudinal tower top load $F_x$ and horizontal bending moment $M_y$ are showing a decreasing trend while the maximum tower top load $F_y$ in lateral direction increases when the environmental condition combined with wind changes from rated to 50-year extreme sea state for the new FWAP without or with nets. As shown in Figs. 47 and 49, when the new FWAP undergoes rated sea state, the maximum values of 1216.37 kN and 1179.43 kN can be detected for $F_x$ without and with nets while the

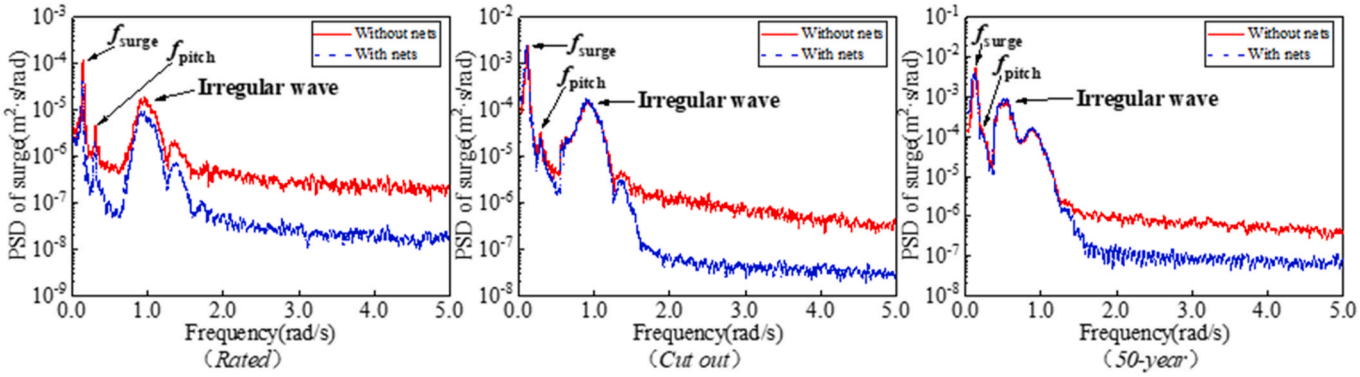


**Fig. 38.** Power spectra of surge response of the new FWAP under combined wind and wave.

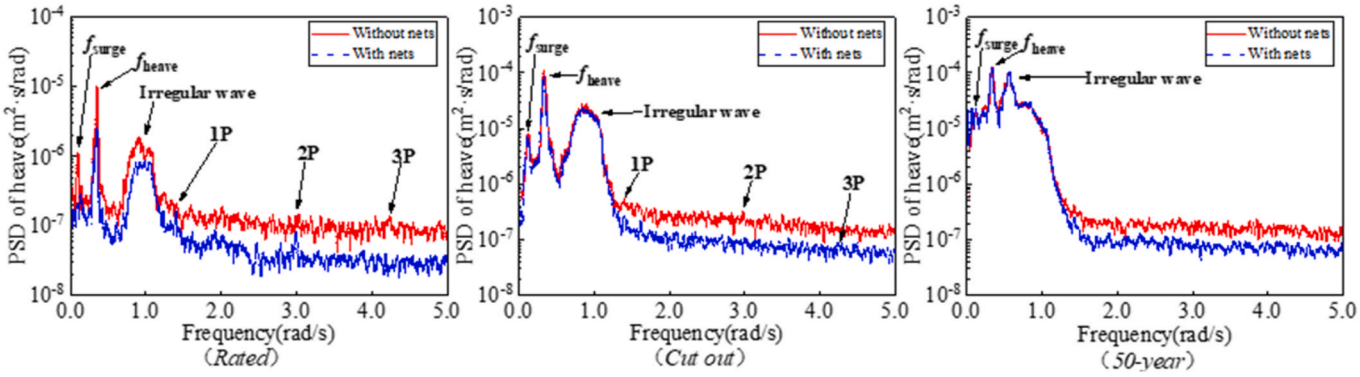


**Fig. 39.** Power spectra of heave response of the new FWAP under combined wind and wave.

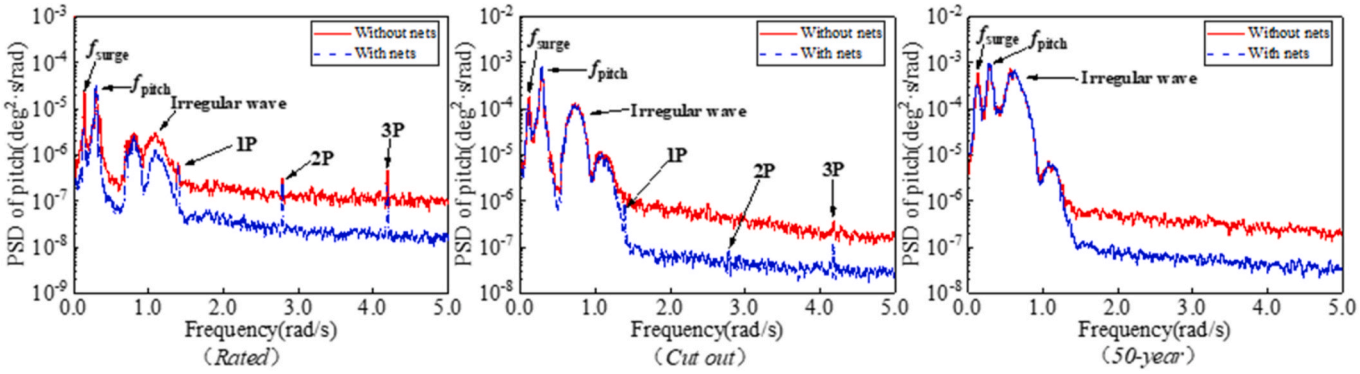


**Fig. 40.** Power spectra of pitch response of the new FWAP under combined wind and wave.

maximum horizontal bending moments are equal to 11506.4 kN•m and 9336.46 kN•m respectively. Compared with those under rated sea state, the maximum values of $F_x$ and $M_y$ under 50-year extreme sea state decrease to 181.03 kN and 2297.33 kN•m without nets as well as 209.38 kN and 4943 kN•m with nets. Unlike $F_x$ and $M_y$, the maximum $F_y$ without and with nets are 139.97 kN and 134.22 kN under rated sea state, and its maximum value is increased up to 1034.97 kN and 901.05 kN under 50-year extreme sea state.

The notable decrease of $F_x$ and $M_y$ can be attributed to the variation of thrust force induced by wind. Under rated sea state combined with wind, the wind turbine rotates normally, leading to large thrust force on the new FWAP. As the oceanic condition is changed to cut out sea state combined with wind, the thrust force induced by wind is reduced due to the variable pitch of wind blades compared with that under rated sea stated. When the new FWAP is subjected to 50-year extreme sea state, the wind turbine stops rotating. Therefore, small thrust force can be detected under this circumstance, leading to the low values of maximum $F_x$ and $M_y$. As for the lateral tower top load $F_y$, since the wind direction is along the $X$ axis, it is seldom affected by thrust force induced by wind. Hence, the maximum $F_y$ is mainly determined by wave loads under different sea states. Consequently, the maximum values of $F_y$ is observed under 50-year extreme sea state, which can be ascribed to the large wave load.

Similarly, nets can also exert a damping or excitation effect on tower top loads of the new FWAP. The damping effect can be detected for $F_x$ and $M_y$ under rated sea state. But when the new FWAP undergoes 50-year extreme sea state, the maximum values of $F_x$ and $M_y$ are increased, indicating the excitation impact of nets. As shown in Figs. 47 and 49, the maximum $F_x$ and $M_y$ without nets are 1216.37 kN and 11506.4 kN•m under rated sea state. While nets are included, the

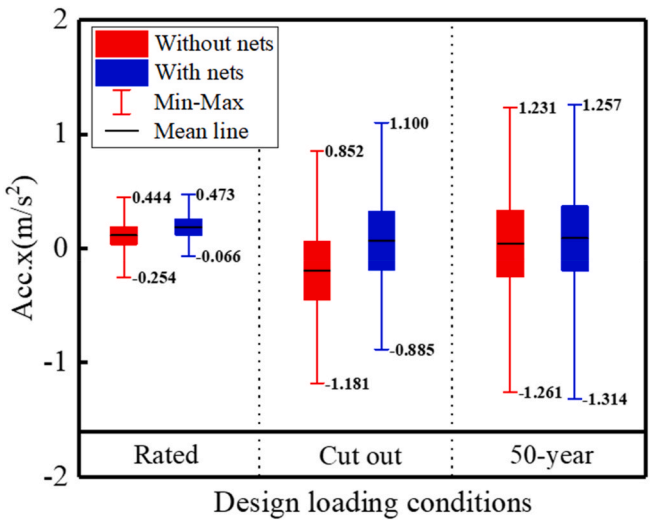


**Fig. 41.** Longitudinal accelerations of the new FWAP under combined wind and wave.

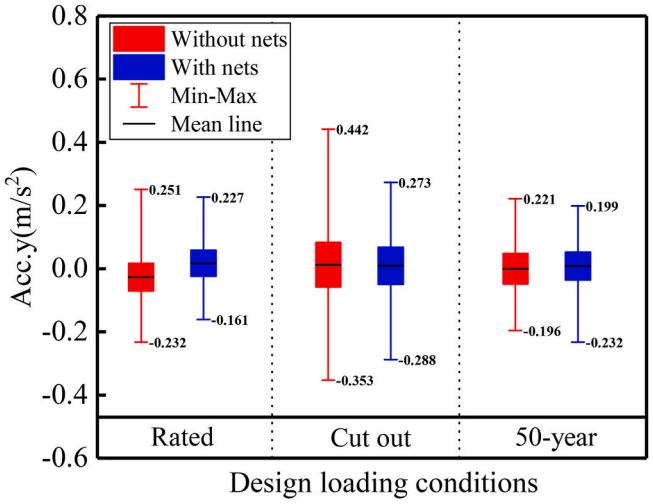


**Fig. 42.** Lateral accelerations of the new FWAP under combined wind and wave.

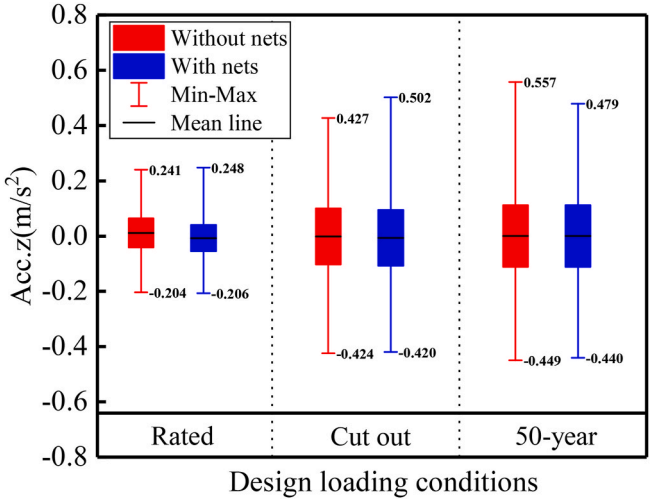


**Fig. 43.** Vertical accelerations of the new FWAP under combined wind and wave.

maximum values of $F_x$ and $M_y$ are decreased to 1179.43 kN and 9336.46 kN•m. By contrast, the maximum $F_x$ and $M_y$ under 50-year extreme sea state are increased from 181.03 kN to 2297.33 kN•m to 209.38 kN and 4943 kN•m when nets are considered. In terms of $F_y$, nets have an excitation effect under rated and cut out sea states. However, the maximum $F_y$ is restrained by nets under 50-year extreme sea state.

The power spectra of the tower top load of the new FWAP without or with nets under combined wind and wave are displayed in Figs. 50–52. Under all three sea states, multi frequency response can be detected for the longitudinal tower top load $F_x$, lateral tower top load $F_y$ and horizontal bending moment $M_y$. Similar to motions and accelerations of the new FWAP, regardless of nets, the frequency peaks induced by motions and irregular wave can be evidently observed under rated, cut out and 50-year extreme sea states. Besides, the power spectra corresponding to tower vibration and rotation of the wind turbine also occur. Noteworthy is that the frequency peaks incurred by the tower vibration and rotation of the wind turbine are more notable compared with those of motions and accelerations, particularly under rated and cut out sea states. As shown in Figs. 50 and 52, the first mode tower vibration in fore-aft direction $f_{FA}^1$ and wind turbine 1P, 2P and 3P excitations are detected for $F_x$ and $M_y$ while there exist the first mode tower vibration frequency in side-side direction $f_{SS}^1$ and wind turbine 1P, 2P and 3P excitations for $F_y$ of the new FWAP without or with nets under rated and cut out sea states. Moreover, the energy allocated on the power spectra of the first mode tower vibration and wind turbine 1P, 2P and 3P excitations is remarkable compared with those of motions and accelerations. When the new FWAP without or with nets is subjected to 50-year extreme sea state, wind turbine 1P, 2P and 3P excitations disappear due to the lack of wind turbine rotation. The frequency peaks $f_{FA}^1$ and $f_{SS}^1$ corresponding to first mode tower vibration in fore-aft and side-side directions are weakened, which can also be attributed to the nonrotation of wind turbine. Meanwhile, the power spectra induced by irregular wave are enhanced due to the enlargement of wave loads. It should also be noticed that the effect of nets on $F_x$, $F_y$ and $M_y$ is not notable under combined wind and wave sea state.

## 5. Discussion

Based on the experimental results, it can be found that when the new FWAP without or with nets undergoes only irregular wave, the wave loads exerted on the FWAP are notably changed under rated, cut out and 50-year extreme sea states, which can be demonstrated by the variation of motions, accelerations and tower top loads. As the oceanic condition changes to 50-year extreme sea state, the accordant wave load is enlarged remarkably, resulting in the evident increase of maximum motions, accelerations and tower top loads of the new FWAP regardless of nets. Besides, there exist notable power spectra induced by irregular wave for the response of motions, accelerations and tower top loads. The tower top vibration can be triggered under only irregular wave, which can be manifested in the power spectra of accelerations and tower top loads of the new FWAP. Meanwhile, the results also prove that the tower top vibration can exert an evident impact on accelerations and tower top loads but not on motions of the new FWAP without or with nets under rated, cut out and 50-year extreme sea states.

Compared with those under only irregular wave, the dynamic behaviors of the new FWAP without or with nets are more complicated when wind and irregular wave are considered simultaneously. As the new FWAP without or with nets undergoes combined wind and wave, the maximum values of motions, accelerations and tower top loads show an increasing or decreasing trend under rated, cut out and 50-year extreme sea states. Similar to those under only regular wave, the maximum values of motions, accelerations in longitudinal and vertical directions as well as lateral tower top load increase notably when the environmental condition combined with wind is changed to 50-year extreme sea state. However, due to the existence of wind, the chang-

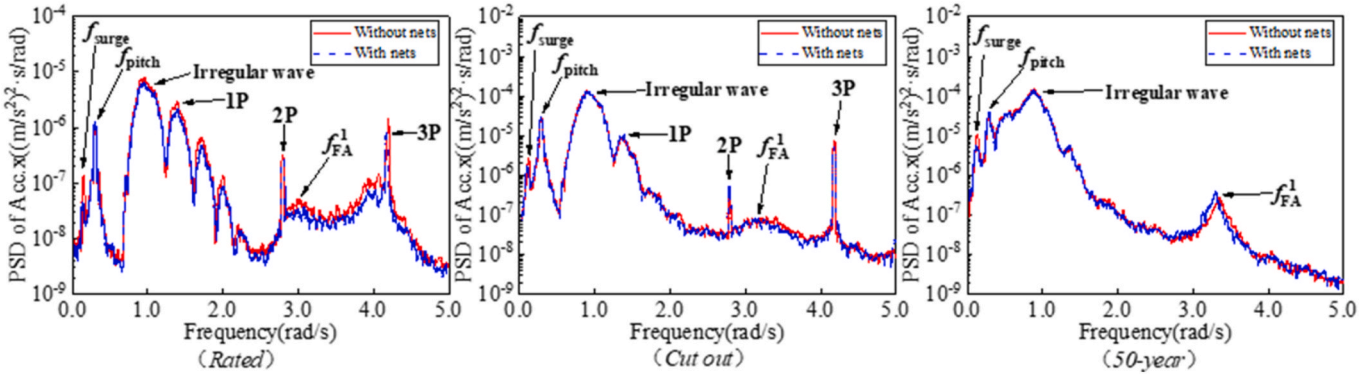


**Fig. 44.** Power spectra of longitudinal accelerations of the new FWAP under combined wind and wave.

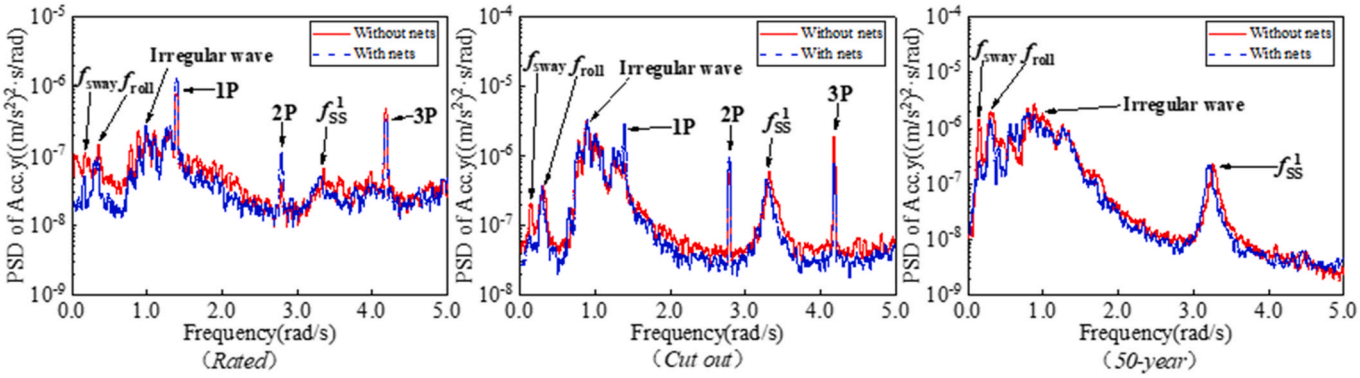


**Fig. 45.** Power spectra of lateral accelerations of the new FWAP under combined wind and wave.

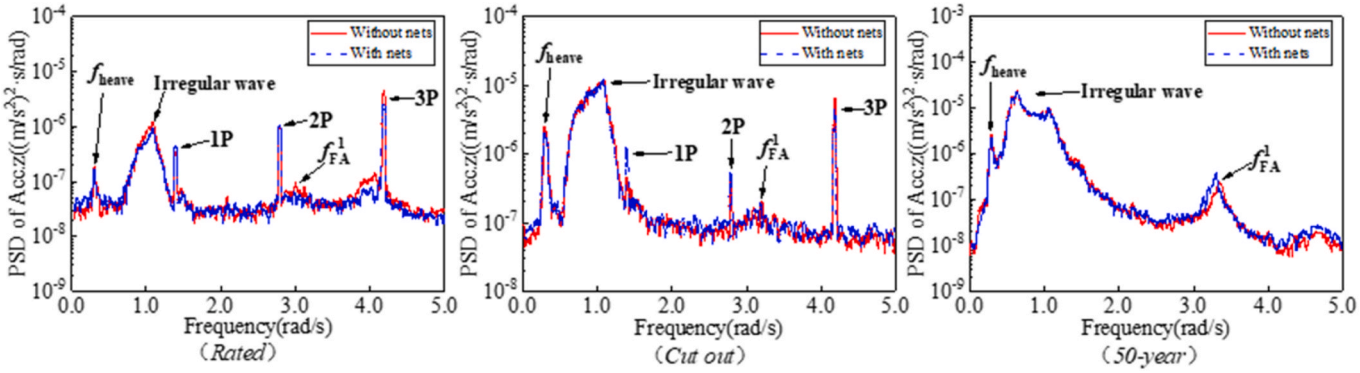


**Fig. 46.** Power spectra of vertical accelerations of the new FWAP under combined wind and wave.

ing trends of lateral acceleration Acc.y, longitudinal tower top load $F_x$ and horizontal bending moment $M_y$ under different sea states are not same as those under only irregular wave. Since there exists the rotation of wind turbine under rated and cut out sea states, the corresponding thrust force due to wind is generated and exerted on the new FWAP. As a result, dynamic responses of the new FWAP without or with nets are affected. Therefore, motions, accelerations and tower top loads are enlarged remarkedly when the environmental condition combined with wind changes from rated to cut out sea state. When the new FWAP is subjected to 50-year extreme sea state, the rotation of wind turbine is forbidden, resulting in the disappearance of thrust force. As the wave load exerted on the new FWAP is notably increased, some responses such as motions, Acc.x, Acc.z and $F_y$ are still amplified in our test, indicating that wave load affects these dynamic responses predominantly under this circumstacne. Meanwhile, it is detected that the maximum values of Acc.y, $F_x$ and $M_y$ are reduced under 50-year extreme sea state compared with those under cut out sea state, which can be attributed to the absence of wind.

Noteworthy is that although the variation trend of some dynamical behaviors under combined wind and wave is similar to those under only irregular wave, the maximum values of motions, accelerations and tower top loads of the new FWAP without or with nets under these two oceanic conditions are almost in different magnitudes. That is, the responses under combined wind and wave are one or several orders of magnitude larger than those under only irregular wave, which indicates that the wind can exert a remarkable effect on the dynamical behaviors of the new FWAP. For example, it can be seen that the increasing rate of surge and pitch of the new FWAP can be up to 352% and 160% without nets as well as 516% and 366% with nets under rated sea state when wind is considered. Moreover, the maximum values of the longitudinal

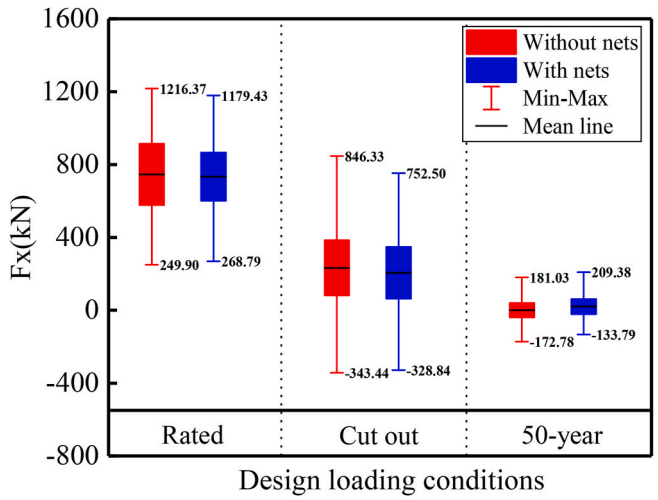


**Fig. 47.** Longitudinal tower top loads of the new FWAP under combined wind and wave.

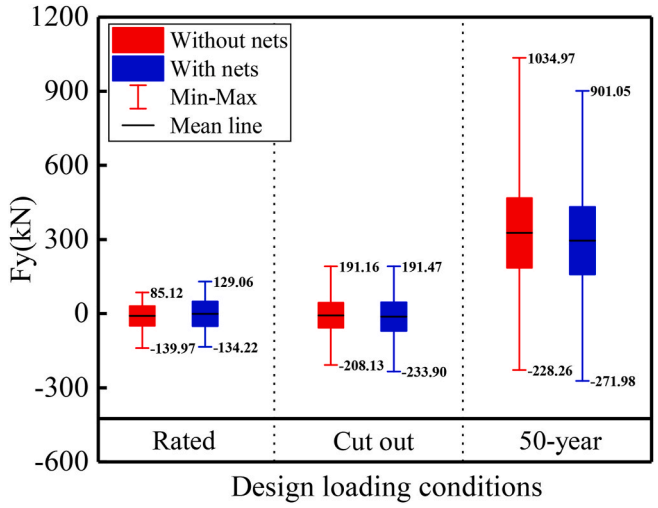


**Fig. 48.** Lateral tower top loads of the new FWAP under combined wind and wave.

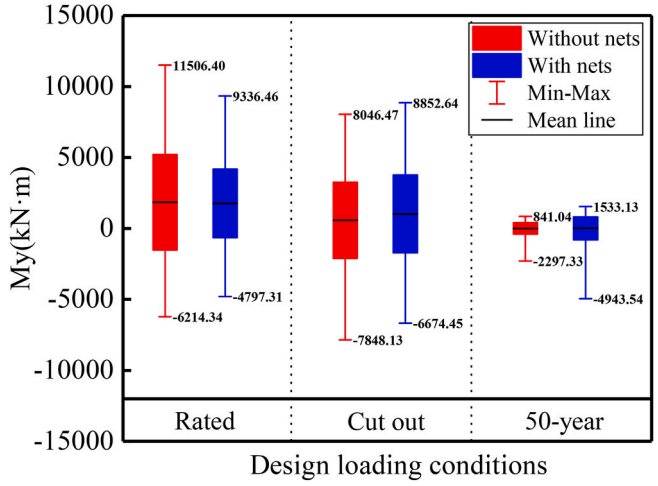


**Fig. 49.** Horizontal bending moments of the new FWAP under combined wind and wave.

tower top load $F_x$ and horizontal bending moment $M_y$ under rated sea state are remarkably increased from 124 kN to 202.3 kN•m up to 1216.37 kN and 11506 kN•m when the new FWAP without nets undergoes combined wind and wave. Additionally, the dynamic responses of the FWAP without or with nets can be more complicated due to the rotation of wind turbine induced by wind, which can be demonstrated in the power spectra of motions, accelerations and tower top loads. And frequency peaks related to wind turbine rotation can be clearly detected. Therefore, it can be concluded that the dynamic responses of the new FWAP regardless of nets can be notably affected by wind, which should be considered and examined during design.

When nets are included in the new FWAP, a damping or excitation effect can be exerted on the dynamical behaviors. It should mention that nets mainly act as a damping factor for the dynamic responses of the new FWAP subjected to only irregular wave. However, both damping and excitation effects of nets can be observed for the responses of the new FWAP when combined wind and wave are considered under different sea states.

## 6. Conclusions

In this study, the dynamical behaviors of an innovative semi-submersible floating wind turbine with aquaculture cage are explored and investigated under rated, cut out and 50-year extreme sea states. Model tests of the new FWAP with scale of 1:40 are mainly carried out in Shanghai Jiao Tong University wind/wave ocean engineering basin. The physical model is well examined and fabricated before the implementation of the experiments. Correspondingly, the motions, accelerations and tower top loads of the new FWAP without or with nets are mainly analyzed and discussed under irregular wave as well as combined wind and wave. Meanwhile, the effect of nets on the dynamic responses of the new FWAP is also studied under different sea states.

Firstly, the free decay and white noise waves tests are conducted, wherein the periods and RAOs of motions can be obtained. Besides, the existence of nets is proved to have an effect on the system period, damping and RAOs of motion.

The experimental results under only irregular wave prove that regardless of nets, the maximum values of motions, accelerations and tower top loads are notably enlarged when the environmental condition changes from rated sea state to 50-year extreme sea state, which can be attributed to the increase of wave loads. For motions of the new FWAP, the maximum surge of 4.544 m occurs with the existence of nets while the maximum values of heave and pitch are 1.411 m and 3.131° with the absence of nets. Similarly, the longitudinal and lateral accelerations Acc.x and Acc.y with the maximum values of 1.333 m/s$^2$ and 0.241 m/s$^2$ respectively can be detected with the consideration of nets for the new FWAP. The maximum vertical acceleration Acc.z of 0.538 m/s$^2$ appears without nets. Nevertheless, the maximum values of the tower top loads $F_x$, $F_y$, and $M_y$ are observed when the nets are not considered, which are equal to 681.7 kN, 90.28 kN and 1416 kN•m respectively. Moreover, multi power spectra corresponding to the motion, irregular wave as well as tower top vibration can be detected under different sea states. A damping effect can be observed on the dynamic responses of the new FWAP due to presence of nets.

When the FWAP without or with nets undergoes combined wind and wave, more complicated dynamic responses can be captured. Since wind loads are exerted on the new FWAP, the maximum values of motions, accelerations and tower top loads are significantly enhanced compared with those under only irregular wave. It can be observed that the maximum surge of 6.322 m is almost 139% as that under only irregular wave, which also appears with the presence of nets. The maximum values of heave and pitch are detected 96% and 112% as those exposed to only irregular wave when nets are not included. For accelerations of the new FWAP, the maximum Acc.x of 1.314 m/s$^2$ occurs with the presence of nets while the maximum Acc.y and Acc.z with values of 0.442 m/s$^2$ and 0.557 m/s$^2$ can be captured due to the net absence.

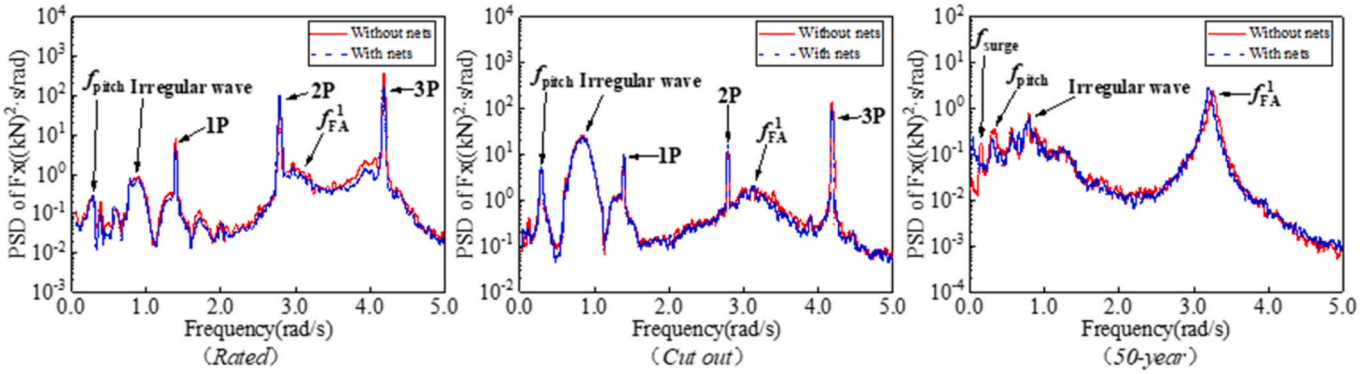


**Fig. 50.** Power spectra of longitudinal tower top loads of the new FWAP under combined wind and wave.

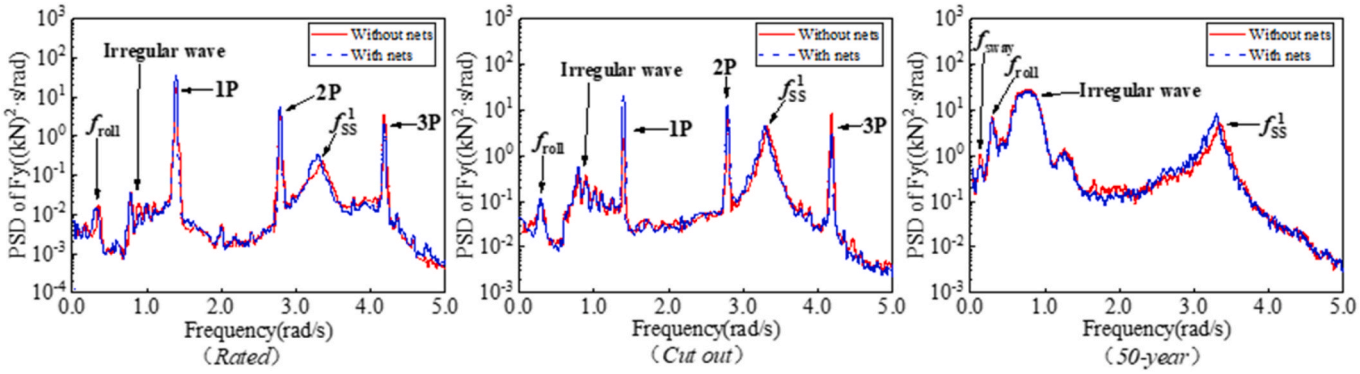


**Fig. 51.** Power spectra of lateral tower top loads of the new FWAP under combined wind and wave.

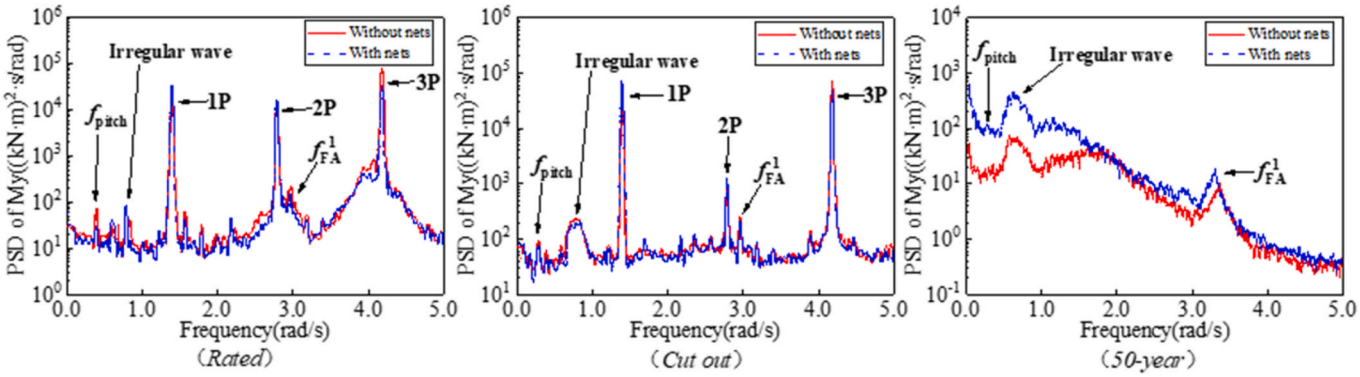


**Fig. 52.** Power spectra of horizontal bending moments of the new FWAP under combined wind and wave.

Among them, the maximum value of Acc.y is increased significantly up to 183% as that under only irregular wave. Note that all the maximum values of tower top loads appear without the existence of nets. The maximum values of $F_x$, $F_y$, and $M_y$ are equal to 1216.37 kN, 1034.97 kN and 11506.40 kN•m respectively, which are 178%, 1146% and 813% as those under only irregular wave. As the oceanic condition changes from rated to 50-year extreme sea state, most responses show a similar changing trend with those under only irregular wave while there also exist notable decrease for accelerations and tower top loads. This reduction can be explained by the nonrotation of wind turbine due to the absence of wind under 50-year extreme sea state. Furthermore, in addition to the frequency components incurred by motion, irregular wave and tower vibration, the frequency peaks of 1P, 2P and 3P excitations accordant to the rotation of wind turbine can be captured in the power spectra of the new FWAP without or with nets, indicating the effect of the wind turbine on the dynamical behaviors of the new FWAP. Under combined wind and wave, the existence of nets can act as a damping or excitation factor on the motions, accelerations and tower top loads.

Although these conducted experimental results can be utilized to improve the innovatively designed FWAP, there still remain many challenges before the new FWAP is put into service, such as the effect of combined wind and wave direction, the consideration of current, the possible wave slamming effect on FWAP, etc. Therefore, the dynamical behaviors of the new FWAP under more complicated conditions required to be investigated in future.

## CRediT authorship contribution statement

**Shugang Cao:** Conceptualization, Methodology, Investigation,

Software, Validation, Data curation, Visualization, Writing – original draft, preparation, Writing – review & editing. **Youliang Cheng:** Conceptualization, Methodology, Supervision, Visualization. **Jinlong Duan:** Supervision, Data curation, Visualization, Writing – original draft, preparation, Writing – review & editing. **Xiaoxu Fan:** Conceptualization, Methodology.

## Declaration of competing interest

The authors declare that they have no known competing financial interests or personal relationships that could have appeared to influence the work reported in this paper.

## Data availability

The data that has been used is confidential.

## Acknowledgement

The work is supported by China Energy Group Key Science and Technology Projects (GJNY-20-17, GJNY-22-13), the National Natural Science Foundation of China (Grants 12202455 and 12132018) and the Strategic Priority Research Program of the Chinese Academy of Sciences (Grant XDA22040304). The authors would like to express their gratitude to the team of Prof. Yongsheng Zhao and the team of Prof. Yuwang Xu at Shanghai Jiao Tong University for their related work and help in the model test process of this project.

## References

[1] F.G. Nielsen, T.D. Hanson, B. Skaare, in: Integrated Dynamic Analysis of Floating Offshore Wind turbines[C]//International Conference on Offshore Mechanics and Arctic Engineering, vol. 47462, 2006, pp. 671–679.
[2] G.R. Tomasicchio, F. D'Alessandro, A.M. Avossa, et al., Experimental modelling of the dynamic behaviour of a spar buoy wind turbine[J], Renew. Energy 127 (2018) 412–432.
[3] D. Roddier, C. Cermelli, A. Aubault, et al., WindFloat: a floating foundation for offshore wind turbines[J], J. Renew. Sustain. Energy 2 (3) (2010), 033104.
[4] H. Li, E.E. Bachynski, Experimental and numerical investigation of nonlinear diffraction wave loads on a semi-submersible wind turbine[J], Renew. Energy 171 (2021) 709–727.
[5] W.Y. Hsu, R.Y. Yang, F.N. Chang, et al., Experimental study of floating offshore platform in combined wind/wave/current environment[J], Int. J. Offshore Polar Eng. 26 (2016) 125–131, 02.
[6] Y. Liu, C. Hu, M. Sueyoshi, et al., Motion response prediction by hybrid panel-stick models for a semi-submersible with bracings[J], J. Mar. Sci. Technol. 21 (4) (2016) 742–757.
[7] Y. Liu, C. Hu, M. Sueyoshi, et al., Motion response characteristics of a Kyushu-University semi-submersible floating wind turbine with trussed slender structures: experiment vs. numerical simulation[J], Ocean Eng. 232 (2021), 109078.
[8] K. Rajeswari, S. Nallayarasu, Experimental and numerical investigation on the suitability of semi-submersible floaters to support vertical axis wind turbine[J], Ships Offshore Struct. 17 (8) (2022) 1743–1754.
[9] A.J. Goupee, B.J. Koo, R.W. Kimball, et al., Experimental comparison of three floating wind turbine concepts[J], J. Offshore Mech. Arctic Eng. 136 (2) (2014).
[10] B.J. Koo, A.J. Goupee, R.W. Kimball, et al., Model tests for a floating wind turbine on three different floaters[J], J. Offshore Mech. Arctic Eng. 136 (2) (2014).
[11] H.R. Martin, R.W. Kimball, A.M. Viselli, et al., Methodology for wind/wave basin testing of floating offshore wind turbines[J], J. Offshore Mech. Arctic Eng. 136 (2) (2014).
[12] H.R. Martin, Development of a Scale Model Wind Turbine for Testing of Offshore Floating Wind Turbine Systems [Master's Thesis], The University of Maine, 2011.
[13] A.N. Robertson, J.M. Jonkman, A.J. Goupee, et al., in: Summary of Conclusions and Recommendations Drawn from the DeepCwind Scaled Floating Offshore Wind System Test campaign[C]//International Conference on Offshore Mechanics and Arctic Engineering, vol. 55423, American Society of Mechanical Engineers, 2013, V008T09A053.
[14] Y. Nihei, K. Iijima, M. Murai, et al., in: A Comparative Study of Motion Performance of Four Different FOWT Designs in Combined Wind and Wave loads [C]//International Conference on Offshore Mechanics and Arctic Engineering, vol. 45493, American Society of Mechanical Engineers, 2014, V007T05A025.
[15] Y. Nihei, H. Fujioka, Motion characteristics of TLP type offshore wind turbine in waves and wind[C], Int. Conf. Offshore Mech. Arctic Eng. 49118 (2010) 283–292.
[16] R. Zamora-Rodriguez, P. Gomez-Alonso, J. Amate-Lopez, et al., in: Model Scale Analysis of a TLP Floating Offshore Wind turbine[C]//International Conference on Offshore Mechanics and Arctic Engineering, vol. 45547, American Society of Mechanical Engineers, 2014, V09BT09A016.
[17] F. Duan, Z. Hu, J.M. Niedzwecki, Model test investigation of a spar floating wind turbine[J], Mar. Struct. 49 (2016) 76–96.
[18] F. Duan, Z. Hu, G. Liu, et al., Experimental comparisons of dynamic properties of floating wind turbine systems based on two different rotor concepts[J], Appl. Ocean Res. 58 (2016) 266–280.
[19] A. Aubault, M. Alves, A. Sarmento, et al., Modeling of an oscillating water column on the floating foundation WindFloat[C], Int. Conf. Offshore Mech. Arctic Eng. 44373 (2011) 235–246.
[20] A. Peiffer, D. Roddier, A. Aubault, Design of a point absorber inside the WindFloat structure[C], Int. Conf. Offshore Mech. Arctic Eng. 44373 (2011) 247–255.
[21] C. Michailides, C. Luan, Z. Gao, et al., in: Effect of Flap Type Wave Energy Converters on the Response of a Semi-submersible Wind Turbine in Operational conditions[C]//International Conference on Offshore Mechanics and Arctic Engineering, vol. 45547, American Society of Mechanical Engineers, 2014, V09BT09A014.
[22] C. Michailides, Z. Gao, T. Moan, Experimental and numerical study of the response of the offshore combined wind/wave energy concept SFC in extreme environmental conditions[J], Mar. Struct. 50 (2016) 35–54.
[23] L. Wan, Z. Gao, T. Moan, et al., Experimental and numerical comparisons of hydrodynamic responses for a combined wind and wave energy converter concept under operational conditions[J], Renew. Energy 93 (2016) 87–100.
[24] N. Ren, Z. Ma, B. Shan, et al., Experimental and numerical study of dynamic responses of a new combined TLP type floating wind turbine and a wave energy converter under operational conditions[J], Renew. Energy 151 (2020) 966–974.
[25] M. Kamarlouei, J.F. Gaspar, M. Calvario, et al., Experimental study of wave energy converter arrays adapted to a semi-submersible wind platform[J], Renew. Energy 188 (2022) 145–163.
[26] SALMAR, Offshore Fish Farming, 2021. https://www.salmar.no/en/offshore-fish-farming-a-new-era. (Accessed 20 February 2003).
[27] X.Y. Zheng, Y. Lei, Stochastic response analysis for a floating offshore wind turbine integrated with a steel fish farming cage[J], Appl. Sci. 8 (8) (2018) 1229.
[28] Y. Lei, S.X. Zhao, X.Y. Zheng, et al., Effects of fish nets on the nonlinear dynamic performance of a floating offshore wind turbine integrated with a steel fish farming cage[J], Int. J. Struct. Stabil. Dynam. 20 (2020), 2050042, 03.
[29] Y. Lei, X.Y. Zheng, H. Zheng, in: Dynamic Analysis of a Floating Offshore Wind Turbine Integrated with a Steel Fish Farming Cage[C]//The 30th International Ocean and Polar Engineering Conference, OnePetro, 2020.
[30] Y. Lei, X.Y. Zheng, W. Li, et al., Experimental study of the state-of-the-art offshore system integrating a floating offshore wind turbine with a steel fish farming cage [J], Mar. Struct. 80 (2021), 103076.
[31] Y.I. Chu, C.M. Wang, Hydrodynamic response analysis of combined spar wind turbine and fish cage for offshore fish farms[J], Int. J. Struct. Stabil. Dynam. 20 (2020), 2050104, 09.
[32] Y.I. Chu, C.M. Wang, H. Zhang, A frequency domain approach for analyzing motion responses of integrated offshore fish cage and wind turbine under wind and wave actions[J], Aquacult. Eng. (2022), 102241.
[33] H.D. Zheng, X.Y. Zheng, Y. Lei, et al., Experimental validation on the dynamic response of a novel floater uniting a vertical-axis wind turbine with a steel fishing cage[J], Ocean Eng. 243 (2022), 110257.
[34] M.J. Fowler, R.W. Kimball, D.A. Thomas III, et al., in: Design and Testing of Scale Model Wind Turbines for Use in Wind/wave Basin Model Tests of Floating Offshore Wind turbines[C]//International Conference on Offshore Mechanics and Arctic Engineering, vol. 55423, American Society of Mechanical Engineers, 2013, V008T09A004.
[35] DNVGL-RP-0286, Coupled Analysis of Floating Wind turbines[S], DNV GL AS, Oslo, Norway, 2019.
[36] DNVGL-RP-C205, Environmental Conditions and Environmental loads[S], DNV GL AS, Oslo, Norway, 2019.